Erasmus University Rotterdam

Econometrics and Management Science
Quantitative Finance

Master's Thesis

Identifying Systematic Risk in Banking Systems

A Graphical Model Analysis

Submitted by: W.F. van Driel (425342)

Supervisor: Dr. M. Grith

Second assessor: Dr. P. Wan

Date: April 12, 2021

Abstract

The outcomes of the financial crisis of 2007-2008 uncovered the flaws in the monitoring of systemic risk in the banking sector, which led to substantial economic loss around the world. This paper explores whether daily equity returns can reflect the dependence structure between banks. Incorporating the latest insights in recursive max-linear models and systemic importance measures, we show that most of the risk in the U.S. banking system originates from large banks, as measured by yearly assets, debts and equity. On the other hand, small banks are most vulnerable to incoming risk. We demonstrate that the bottleneck in the system occurs at average sized banks, since a high amount of accumulated risk flows through these banks to the smaller banks. This indicates that saving the former banks could stop contagion at an early stage. The viability of these results is confirmed using monthly and excess returns, and several hyper-parameter sets. As a whole, we suggest that recursive max-linear models and systemic importance measures can be combined to develop an early warning system, which reduces contagion across the banking system.

Keywords: extreme value theory, max-linear models, systematic risk, causal order

JEL Classification: C14, C58, G21, G32

Contents

1 Introduction

The modern banking system represents a complex network of mutual credit relations. These dependencies are often seen as the driving factor behind the global financial crisis of 2007, where the failure of one institution might cause a domino effect. The most vivid example is the collapse of the US investment bank Lehman Brothers in 2008, after which banks were no longer able to acquire liquidity (Georg, 2013). This event unfolded the dramatic effects that systematic risk can have in a banking system. Additionally, the introduction of sophisticated financial products, such as credit default swaps, has increased the complexity of financial dependencies even further, which complicates the investigation of any banking system.

To reveal the hidden structure between banks, previous research largely focuses on financial contagion as the driving factor behind systematic risk, which is the spread of market disturbances caused by co-movements in financial instruments (Allen & Gale, 2000). Within this field there are two strands of literature that have received most attention. The first applies network topology on bank balance-sheet data to represent banks and their interconnections (see e.g. Furfine (2003) and Boss, Elsinger, Summer, and Thurner (2004)). Parallel to their work is another strand of literature that focuses on financial contagion through rare events. In particular, these studies use extreme value theory (EVT) on financial data to quantify the co-movements between banks in times of distress (see e.g. Hartmann, Straetmans, and De Vries (2005) and Zhou (2009)).

Although the aforementioned techniques are well-established, they are mostly applied as two separate entities, whereas their combination could offer a new perspective on financial contagion. The recent introduction of graphical models for extremes serves this idea. Concretely, graphical models are able to perform high-dimensional inference by factorizing their densities into a number of low-dimensional models. This allows for making casual inference and probabilistic modeling under sparsity constraints, such that an explicit network can be constructed and traditional centrality measures can be applied (Engelke & Ivanovs, 2020).

A recent study in this field is conducted by Klüppelberg and Krali (2021), in which the authors use recursive max-linear (ML) models to uncover causal dependence structures between random variables. These models assume that random variables are defined on a graph, which allows to recursively determine their value based on predecessors and shocks. Despite of their potential to uncover dependence structures during extreme events, they have not yet been applied in the field of financial contagion. We fill this gap by applying graphical models to a banking system, which provides a new perspective on systematic risk. In particular, this paper investigates how recursive ML models on causal inference can be used to uncover the underlying

network for extreme events in the U.S. banking system.

For this reason, we employ the framework of Klüppelberg and Krali (2021) to daily bank equity returns from the New York Stock Exchange (NYSE) between 1990 and 2015. The equity returns are used to model the banking system through a directed acyclic graph (DAG), where every bank is a vertex and its condition (i.e. the level of financial distress) is determined by the returns. We focus on the left tail of the distribution as financial assets tend to display larger degrees of co-movement during periods of distress (Forbes & Rigobon, 2002). The size of each bank is determined using accounting data, such as total assets, debts and equity, over the same sample period.

Next, a scaling technique is used to extract a causality re-ordering that would make the DAG well-ordered, in which case the causal order can be determined. These scalings are estimated based on extreme dependence measures of Cooley and Thibaud (2019). Once the DAG is constructed, several centrality measures such as degrees and betweenness centrality are calculated to give an idea about the relative importance of each bank in the system. These results are related to the systemic importance measures of Zhou (2009) and Segoviano Basurto and Goodhart (2009), and their relation is quantified using various correlation coefficients.

Overall, we find that most large banks influence the economic status of other banks. In fact, large banks do not have a direct impact on each other, but instead cause average sized banks to be the bottlenecks in the system, as they receive and transmit a significant amount of risk. This could make them a potential target for policy makers to cease a domino effect at an early stage. Furthermore, we find that size is positively correlated with the probability that a particular bank causes others to default, which is in in line with existing literature. However, contrary to the findings of Zhou (2009), the probability that a bank defaults due to the default of other banks is negatively correlated with size, which could be due to the acyclic nature of the imposed graph. The viability of the results is confirmed using a variety of robustness checks, including low-frequency data and excess returns, which yield similar but more modest conclusions.

The relevance of this research is twofold. From a scientific point of view, we provide a new perception on the usefulness of graphical models in the context of systematic risk analysis. In fact, we are the first to explain the causal dependence structure between banks using the latest insights of Klüppelberg and Krali (2021), which can provide useful applications in modeling and visualizing systemic risk in the banking system. From a social perspective, the insights derived from the research may be used by financial authorities to model the network structure of banks and identify in what way the risk of financial contagion can be reduced. This is especially important since the economic loss of a financial crisis can take up about 20% of a nation's GDP

within the first few years after the crisis (Valencia, Laeven, et al., 2008).

The remainder of this paper is organized as follows. First, the literature and its relevance to this research are discussed in Section 2. Subsequently, recursive max-linear models and systemic importance measures on directed acyclic graphs are introduced in Section 3. Summary statistics of the data are presented in Section 4, after which the estimation procedures are outlined in Section 5. Next, the results of the analysis are described in Section 6 and their robustness is verified in Section 7. Finally, Section 8 concludes the paper and provides suggestions for future research.

2 Literature review

The literature on systematic risk is vast and spans several decades[1]. In particular, studies on financial contagion as a source of systematic risk have explored complex linkages between institutions as well as the impact they have on the stability of the system. The most well-known work is carried out by Allen and Gale (2000), who analyze the effects of contagion through different network structures. They find that the system is more resilient to withstand individual insolvencies when it is fully-connected. The intuition for this is that an indirect link between two banks can cause contagion, but a direct link is needed for insurance.

Aside from Allen and Gale (2000), the effects of contagion through direct linkages are explored by Freixas, Parigi, and Rochet (2000), Eisenberg and Noe (2001), and Gai and Kapadia (2010)[2]. While Freixas et al. (2000) show that a circular banking system is less resilient to individual insolvencies, the latter two studies apply more complex network structures to analyze which features of a network support contagion. Notably, Gai and Kapadia (2010) use techniques that are traditionally applied in epidemiological research to assess the spread of financial contagion in a banking system. By selecting more advanced networks, they also find that dense networks can bear simultaneous failures, but are more vulnerable to individual shocks (Gai & Kapadia, 2010).

Parallel to the theoretical literature, a stream of empirical analyses is conducted to find evidence of contagious failures resulting from mutual credit liabilities. For example, Furfine (2003) investigates the US banking system, Boss et al. (2004) consider Austria, Upper and Worms (2004) Germany, and Martinez-Jaramillo, Alexandrova-Kabadjova, Bravo-Benitez, and Solórzano-Margain (2014) Mexico. Although their studies provide similar results, which demon-

[1] See De Bandt and Hartmann (2000) and Allen, Babus, and Carletti (2009) for a comprehensive overview of systematic risk modeling.

[2] See Allen and Babus (2009) for a survey on applications that use network topology in banking systems and other financial disciplines.

strate that dense banking systems are robust to large shocks, they yield a too optimistic estimator of financial contagion (Allen et al., 2009). In particular, their results are based on an extremely sensitive estimation procedure of linkages between banks. By including financial derivatives in their model, such as credit default swaps (CDS), the spread of systematic risk could be found to be more severe (Nijskens & Wagner, 2011).

Another approach to identify financial contagion is by investigating the rare events that constitute them. To this end, recent developments on EVT can fill the gap. The idea of EVT is to extrapolate observations beyond the data range and create probability models for the tail of a distribution. Hartmann et al. (2005), Zhou (2009), and De Jonghe (2010) are among the first to apply multivariate EVT within a banking system. In particular, Zhou (2009) uses bank stock returns to relate the size of a bank, measured by accounting data, to its importance in the financial system. To do so, the author applies systemic importance measures of Segoviano Basurto and Goodhart (2009) and extends these with the so-called vulnerability index. Interestingly, it seems that the size of a bank should not be used as a proxy for its importance in the system. Alternatively, systemic importance measures that use CDS spreads can also provide valuable insights in a banking system as shown by Rodríguez-Moreno and Peña (2013).

The recent introduction of graphical models in extreme value statistics might enable us to find a more appropriate proxy for systemic importance. Recent studies by Gissibl and Klüppelberg (2018), Engelke and Hitz (2018), and Segers (2019) show that these models in combination with conditional independence structures can define probabilistic sparsity, since they allow the decomposition of high-dimensional distributions into low-dimensional components. The work by Gissibl and Klüppelberg (2018) is especially noteworthy, introducing recursive max-linear models that are defined on a DAG. In a follow-up study Gissibl, Klüppelberg, and Lauritzen (2019) establish a generalized maximum likelihood estimator for these models, which enables to learn the graph structure from empirical data. Although this estimator shows promising results, we do not use it in this paper. Instead, we focus on the non-parametric estimator of Klüppelberg and Krali (2021), which combines well-known aspects of EVT with graph theory. Overall, max-linear models serve the purpose of our research well, as they have the ability of uncovering the causal dependence between variables.

Further research in graphical models includes Einmahl, Kiriliouk, and Segers (2018) who demonstrate that a recursive max-linear model is able to uncover the dependence structure of the EURO STOXX 50 Index, Gnecco, Meinshausen, Peters, and Engelke (2019) who propose an algorithm for learning causal dependence structures in extremes, and Buck and Klüppelberg (2020) who introduce propagating noise models that are estimated using minimum ratios. We

refer to Engelke and Ivanovs (2020) for more discussions and the latest insights in this field.

The aforementioned papers illustrate that graphical models in extreme value statistics can uncover dependence structures in different network architectures. We extend the literature on contagion by examining whether these models can be applied to modeling systematic risk in banking systems. To do so, we will apply the new non-parametric algorithm for recursive max-linear models by Klüppelberg and Krali (2021) to US banking data, which allows to find the causal order of the banks through a new scaling technique. This is closely related to the systemic importance measures of Segoviano Basurto and Goodhart (2009) and Zhou (2009), because the latter measures also allows for a ranking in terms of significance of each bank to systematic risk during financial distress.

3 Methodology

This section introduces the methods for uncovering the causal dependence structure in a banking system. The max-linear models that are used throughout this paper are introduced in Section 3.2. Subsequently, the tail coefficients that capture the dependence structure are derived in Section 3.3, after which the investigation of the causal order is explained in Section 3.4. Several centrality measures, which describe the relative importance of a vertex, are mentioned in Section 3.5. Finally, three systemic importance measures are described in Section 3.6

3.1 Directed acyclic graphs

This paper applies graph theory on financial data to model the banking system, where the vertices represent banks and the edges the causal dependence structure from one bank to another. More specifically, we assume that the graph contains directed edges and has no directed cycles. This particular graph is called a DAG and is denoted by $\mathcal{D} = (V, E)$ with vertices $V = \{1, \dots, d\}$ and edges $E = \{(v, u) : u \in V \text{ and } v \in \text{pa}(u)\}$, where $\text{pa}(u)$ are adjacent vertices that immediately precede vertex v. We formally refer to these vertices as the parents of vertex v. Every vertex has a parent except the root vertex, in which case $\text{pa}(u) = \emptyset$.

Following the notation of Klüppelberg and Krali (2021), we define $\text{an}(u)$ as the ancestors of vertex u, which are all vertices from which it is possible to end up in u through a path. Similarly, we denote $\text{An}(u)$ as the ancestors of u including the vertex itself; that is, $\text{An}(u) = \text{an}(u) \cup \{u\}$. A path from vertex v to u is given by $p_{vu} = [k_0 = v \to l_1 \to \cdots \to k_m = u]$, which has length $|p_{vu}| = m$. All possible paths between these vertices are collected in the set P_{vu}. It is important to note that each vertex $u \in V$ represents the realization of a random variable X_u, and the dependence between two random variables can be represented through an edge connecting the

corresponding vertices.

Finally, the random vector $\boldsymbol{X} = (X_u : u \in V)$ contains financial data of every bank in the system. Since the focus of this research lies on distress situations, it should hold that such situations result in large values of $\boldsymbol{X}_u$. That is why it is assumed that the random vector contains the loss of equity returns for every bank. To link the financial series in a natural manner to the graph, it is assumed that the DAG is well-ordered; that is, for all $u \in V$, it must hold that $u < v$ if $v \in \text{pa}(u)$. We refer to Table A.1 in Appenidx A for a compact overview of the mathematical notation that is used throughout this paper.

3.2 Recursive max-linear models

This paper builds on the causality and estimation methods of Klüppelberg and Krali (2021) that takes extremes into account. It is assumed that the relationship between each vertex can be captured by a specific class of recursive structural equation models (recursive SEMs), that identify every vertex through its parent vertices and innovations. More specifically, the causal models consist of a set of equations that are of the form

$$X_u = f_u\left(\text{pa}(u), \varepsilon_u\right) , \qquad u \in V , \tag{3.1}$$

where $f_u(\cdot)$ is some non-linear function and $(\varepsilon_u : u \in V)$ are innovations that capture omitted factors. Gissibl and Klüppelberg (2018) propose a max-linear specification of $f_u(\cdot)$ in the context of extreme risk analysis, which has as an advantage that it can statistically capture possible dependence structures between variables even if their dimension is large.

The notion of max-linearity refers to selecting the maximum of two linear terms: the weighted influence of a parent vertex and its noise. This results in the so-called max-linear structural equation model $\boldsymbol{X}$ given by

$$X_u = \bigvee_{v \in \text{pa}(u)} c_{uv} X_v \vee c_{uu} \varepsilon_u , \qquad u \in V , \tag{3.2}$$

where $c_{uv} \in \mathbb{R}_+$ is the positive edge weight for $v \in \text{pa}(u)$ and $u \in V$. The operator $\bigvee$ represents the maximum between random variables over a given domain; that is, $\bigvee_{v \in \text{pa}(u)} X_v := \max_{v \in \text{pa}(u)} X_v$. Hence, representation (3.2) is by definition non-linear. Depending on the magnitude of the weights in this representation, they constitute the risk moving from one vertex to another. There are several types of processes which coincides with (3.2), with the most well-known being the max auto-regressive moving average (MARMA), which are thoroughly studied by Davis and Resnick (1989) and Zhang and Smith (2004).

The innovations are assumed to be i.i.d. random variables with support $\mathbb{R}_{>0}$ and atom-free

distributions. These properties imply the existence of a DAG $\mathcal{D}$ which encodes conditional independence relations in the distribution via the (directed global) Markov property (Pearl, 2009). That is, the distribution of $\boldsymbol{X}$ is Markov relative to $\mathcal{D}$. One way of interpreting the innovations is by viewing them as random scalings of edge weights. In fact, Gissibl and Klüppelberg (2018) show that $\boldsymbol{X}$ can be identified through its innovations $\boldsymbol{\varepsilon}$ by performing a path analysis. Consider the path p_{vu} from vertex v to u, and denote $d_{vu}(p) = c_{k_0,k_0} \prod_{l=0}^{m-1} c_{k_l,k_{l+1}}$ as the weight of this path. In that case, $\boldsymbol{X}$ is a recursive max-linear (recursive ML) model and is given by

$$X_u = \bigvee_{v \in \mathrm{An}(u)} b_{uv} \varepsilon_v \,, \qquad u \in V \,, \tag{3.3}$$

where b_{uv} is the ML coefficient defined as

$$b_{uv} = \begin{cases} \bigvee_{p \in P_{vu}} d_{vu}(p) & \text{if } v \in \mathrm{an}(u) \\ c_{uu} & \text{if } v = u \\ 0 & \text{otherwise} \,. \end{cases} \tag{3.4}$$

Note that in this research we are essentially interested in estimating these coefficients, as they represent the max-weighted path from one vertex to another. All coefficients are captured in the ML coefficient matrix $B = (b_{uv})_{u,v=1,\dots,d} \in \mathbb{R}_+^{d \times d}$.

For notational convenience, we refer to the v-th column of B as b_v, for $v \in V$. A prominent example in which the ML coefficient matrix is calculated can be found in Example B.1 in Appendix B. Furthermore, for the sake of simplification, define the matrix-operator $\odot : \mathbb{R}_+^{m \times n} \times \mathbb{R}_+^{n \times p} \to \mathbb{R}_+^{m \times p}$ as $(F \odot G)_{ik} = \bigvee_{j=1}^{m} f_{ij} g_{jk}$ for $i = 1, \dots, n$ and $k = 1, \dots, m$. The matrix operator $\odot$ allows to present representations (3.2) and (3.3) in terms of B as

$$\boldsymbol{X} = B \odot \boldsymbol{\varepsilon} \,. \tag{3.5}$$

This representation contains the full vector $\boldsymbol{X}$, which will be used in the sections hereafter.

3.3 Tail pairwise dependence matrix

So far, we have only assumed that the innovations are i.i.d. random variables. By imposing additional assumptions, the distribution of $\boldsymbol{X}$ on $\mathcal{D}$ can be identified. Specifically, when the innovations $\boldsymbol{\varepsilon}$ are multivariate regularly varying, the extremal dependence structure between vertices can be gauged through a bi-variate measure that contains information about the scaling of $\boldsymbol{X}$ (Cooley & Thibaud, 2019). This subsection summarizes the theory on regular variation and demonstrates how this can be used to obtain the extremal dependence measure.

Roughly speaking, a random vector is multivariate regularly varying (MRV) if its elements jointly share a heavy-tail (Resnick, 2007). A convenient property of a MRV vector is that its

dependence structure can be described by a spectral, or angular, measure $S_{\boldsymbol{X}}$ on the $(d-1)$-dimensional unit ball $\boldsymbol{\Theta}_{d-1} := \left\{\boldsymbol{\theta} \in \mathbb{R}^d : \|\boldsymbol{\theta}\| = 1\right\}$ (Resnick, 2007). A full derivation of this measure is provided in Section A.1 in Appendix A. To obtain the spectral measure, we need to ensure that $\boldsymbol{X}$ itself is MRV; denoted as $\boldsymbol{X} \in \text{MRV}_{\alpha}^{d}$ with tail index $\alpha > 0$. A useful observation of Klüppelberg and Krali (2021) is that the atoms where $S_{\boldsymbol{X}}$ has mass are in fact the normalized columns of B. This means that by standardizing $\boldsymbol{\varepsilon}$ and restricting it to follow a generalized extreme value (GEV) distribution, all scaling information is in the standardized ML coefficient matrix. In this case we ensure that regular variation of the ML model is obtained.

Consequently, we use the following three assumptions on the underlying distribution throughout this paper. First, for mathematical convenience, the ML model is heavy-tailed with tail coefficient $\alpha = 2$. Second, the noise vector $\boldsymbol{\varepsilon} \in \text{MRV}_{2}^{d}$ follows a Fréchet(2) distribution, and has independent and standardized elements. This ensures that the max-linear combinations of independent Fréchet random variables are dense in the class of d-dimensional multivariate extreme value distributions with Fréchet marginal s (Klüppelberg & Krali, 2021). Third, B is standardized, which results in $\boldsymbol{X}$ being standardized. The standardized components ensure that we can later identify the graphical structure, which will be explained thoroughly in Section 3.4.

There are several ways in which the dependence between vertices in the graph can be gauged. Since the focus of this research lies on times of financial distress, a natural choice would be to consider the tails of the distribution where these events occur. Let $(\boldsymbol{\omega}, R)$ be the polar coordinates of $\boldsymbol{X}$ in the unit hypersphere, as defined in Section A.1. Larsson and Resnick (2012) show that by using the aforementioned assumptions in combination with the spectral measure in equation (A.3), it is possible to define the extremal dependence measure between any two vertices in the graph as

$$\sigma_{\boldsymbol{X}_{uv}} = \int_{\boldsymbol{\Theta}_{d-1}} \omega_u \omega_v \, \mathrm{d}S_{\boldsymbol{X}}(\boldsymbol{\omega}) \,, \tag{3.6}$$

where $u, v \in V$ and $\boldsymbol{\omega} \in \boldsymbol{\Theta}_{d-1}$. These bi-variate measures are captured in the tail pairwise dependence matrix (TPDM) $\Sigma_{\boldsymbol{X}} = (\sigma_{\boldsymbol{X}_{uv}})_{u,v=1,\ldots,d} \in \mathbb{R}_{+}^{d \times d}$. Intuitively, $\sigma_{\boldsymbol{X}_{uv}}$ represents the asymptotic dependence between two vertices in $\mathcal{D}$. Recall that in a polar system ω_u represents the direction in which vertex u moves in the unit hypersphere. Hence, $\sigma_{\boldsymbol{X}_{uv}}$ measures to which extent two vertices move in the same direction.

Cooley and Thibaud (2019) demonstrate that the diagonal elements of the TPDM contain details about the scale of the elements of $\boldsymbol{X}$, and that their sum is equal to the total mass of the spectral measure. Using these properties, it is straightforward to calculate the standardized ML coefficients in a well-ordered DAG; particularly since B is standardized. Define for $\boldsymbol{v} \subseteq V$ the maximum over the vector $\boldsymbol{X}$ as $M_{\boldsymbol{v}}$; that is, $M_{\boldsymbol{v}} := \max_{v \in \boldsymbol{v}} X_v$. In that case, Klüppelberg

and Krali (2021) show that the squared scalings in a well-ordered DAG $\mathcal{D}$ can be calculated as

$$\sigma^2_{M_{\boldsymbol{v}}} = \sum_{k=1}^{d} \left(\bigvee_{i \in \boldsymbol{v}} b^2_{ik} \right) . \tag{3.7}$$

However, as most DAGs are not well-ordered, the above relation is incomplete and cannot be used for real-world applications. The following section shows how to overcome this issue.

3.4 Identifying the causal order

Let $\boldsymbol{X}^*$ be a randomly ordered ML model and $V^* := \{1^*, \dots, d^*\}$ the corresponding set of vertices. Klüppelberg and Krali (2021) show that the distribution of $\boldsymbol{X}$ is invariant with respect to column permutations, which allows to consider the B which can have its columns arranged into upper-triangular form via row permutations. Hence, the randomly ordered vector $\boldsymbol{X}$ only needs row permutations to become well-ordered.

Consider the permutation function $\pi : B^* \to B$, which transforms the ML coefficients belonging to a randomly ordered ML model to one that is well-ordered on a DAG $\mathcal{D}$. Redefine the maximum operator as $M_{-m,am} := \max\{X_1, \dots, aX_m, \dots, X_d\}$. According to Theorem 2 of Klüppelberg and Krali (2021), it holds that some vertex $v^* \in V^*$ is the root vertex in a well-ordered DAG $\mathcal{D}$ from a randomly ordered vector $\boldsymbol{X}^*$ if there exists $a > 1$ such that

$$\sigma^2_{M_{-v^*,av^*}} - \sigma^2_{M_V} = a^2 - 1 . \tag{3.8}$$

Similarly, the descendants can be identified by considering a d-tuple maximum over the remaining vertices. More specifically, suppose that we have identified the first h vertices corresponding to $\boldsymbol{h} := \{\pi^{-1}(d), \dots, \pi^{-1}(d-h+1)\}$, and denote the d-tuple maximum as

$$M_{\boldsymbol{h},m^*,k^*} := \max\left\{X_{\pi^{-1}(d)}, \dots, X_{\pi^{-1}(d-h+1)}, X_{m^*}, X_{k^*}\right\} , \tag{3.9}$$

where $k^* \notin \boldsymbol{h} \cup \{m^*\}$ and

$$M_{\boldsymbol{h}_a,m^*_a,k^*} := \max\left\{aX_{\pi^{-1}(d)}, \dots, aX_{\pi^{-1}(d-h+1)}, aX_{m^*}, X_{k^*}\right\} . \tag{3.10}$$

Using these two operators, the vertex $v^* \notin \boldsymbol{h}$ is next in ordering if there exists $a > 1$ such that

$$\sigma^2_{M_{\boldsymbol{h}_a,v^*_a,k^*}} - \sigma^2_{M_V} = (a^2-1)\sigma^2_{M_{\boldsymbol{h},v^*}} . \tag{3.11}$$

The representations above imply an iterative approach for ordering the DAG, which is captured in Algorithms C.1 and C.2 in Appendix C. We refer to Theorem 3 of Klüppelberg and Krali (2021) for a formal derivation of this relationship.

3.5 Centrality measures

Although the methodology of Klüppelberg and Krali (2021) primarily focuses on retrieving the causal order of a network, it also yields the explicit graphical structure of any system. This enables us to use traditional centrality measures from graph theory to identify the most influential vertices within a graph. Note that this idea is not new in the context of financial contagion. For example, Boss et al. (2004), Gai and Kapadia (2010), and Georg (2013) use the in-degree and out-degree of every bank in a network to gauge the risk flowing from one to another. The in-degree of a vertex is the number of incoming edges, whereas the out-degree is the number of outgoing edges. Due to the nature of our methodology, these measures can be used to determine the risk flow.

Another notable centrality measure is betweenness centrality, which determines for every vertex the number of shortest paths that pass through this vertex. Related to our research, the betweenness centrality indicates the bottlenecks in the system. That is, banks with a high betweenness centrality function spread a lot of risk to other banks and by indicating those banks, contagion across the system can be stopped at an early stage. Given that the recursive ML model results in a unilaterally connected graph, there exists at least one shortest path between the vertices such that it is valid to use this measure. Hence, the betweenness centrality for vertex v is given as

$$\gamma(v) = \sum_{u \neq v \neq w} \frac{\lambda_{wu}(u)}{\lambda_{wu}} \qquad u, v, w \in V\,, \tag{3.12}$$

where $\lambda_{wu}(v)$ are the number of shortest paths that start at vertex w, go through vertex v and end at vertex u, and λ_{wu} are the total number of shortest paths.

Typically, these paths are found by minimizing the weights of the edges that are used in each path. However, as mentioned in Section 3.2, the ML coefficients represent the maximum risk moving between vertices. By using these coefficients as edge weights to find the shortest path, we in fact obtain a flow with the least chance of happening. That is why in this setting the weights equal to the inverse of the ML coefficients when they are strictly larger than zero, and zero otherwise.

3.6 Systemic importance measures

Systemic importance measures are traditionally used to evaluate the relative importance of a financial institution in the system. Specifically, they consider a subset of financial data which represents an institution at distress. Zhou (2009) uses these measures to reveal the relation between a bank's size and its systemic importance, and introduces two additional measures: the

SII and VI. There are two main reasons why these measures are appealing to our research. First, it is shown that systemic importance measures can capture the dependence structure between financial institutions well. Second, they are estimated using EVT which makes them comparable to the proposed methodology of Klüppelberg and Krali (2021). In the spirit of Zhou (2009), equity returns are used to display the financial status of each bank.

There are several differences between systemic importance measures and ML models, with the most important being that the latter requires the assumption of regular variation to describe the distribution of the underlying model. Systemic importance measures are more flexible as they only entail a threshold parameter. To illustrate this, consider the first measure proposed by Segoviano Basurto and Goodhart (2009), which evaluates the conditional probability of having at least one additional bank failure, while assuming that another bank fails. We abbreviate this measure by PAO. Following the notation of Zhou (2009), the PAO of a bank i is given by

$$PAO_i(p) = \mathbb{P}\left(\{\exists j \neq i : X_j > VaR_j(p)\} \mid X_i > VaR_i(p)\right) , \tag{3.13}$$

where $VaR_i(p)$ represents the Value at Risk (VaR) at quantile p which is the minimum loss that occurs over a certain period for a given quantile p. The VaR is often used in financial literature and applications, because it is sub-additive in the tail and describes conditional distributions well (Danielsson, Jorgensen, Mandira, Samorodnitsky, & De Vries, 2005).

Another systemic importance measure that uses this risk standard is the systemic impact index (SII). It is closely related to PAO, as they both consider the event that at least one bank fails due to financial distress at the other. However, SII examines the expected number of banks that are infected by the spread of contagion, and can be formulated as

$$SII_i(p) = \mathbb{E}\left(\sum_{j=1}^{d} \mathbb{1}\left\{X_j > VaR_j(p)\right\} \mid X_i > VaR_i(p)\right) , \tag{3.14}$$

where $\mathbb{1}_A$ is an indicator function returning 1 if event A is true, and 0 otherwise.

Although both PAO and SII are informative in a dense banking system, they focus on the impact of one bank's failure on the overall system. It could be, however, equally interesting to consider what the effect of a system failure is on an individual bank. To this end, Zhou (2009) proposes the vulnerability index (VI) which is given by

$$VI_i(p) = \mathbb{P}\left(X_i > VaR_i(p) \mid \{\exists j \neq i : X_j > VaR_j(p)\}\right) . \tag{3.15}$$

A typical problem when estimating the Value-at-Risk at probability level p, where p is close to zero, is that most methods cannot precisely apply statistic inference in the tails of a distribution due to a lack of observations (De Haan & Ferreira, 2007). Consequently, multivariate EVT is used to model the co-movement of extreme events between banks, and by doing so capture the

interdependence structure between the losses of the bank stock returns. A common approach is to model the co-movement of extreme events between banks by defining a characterizing function of the form

$$L(x_1, \ldots, x_d) = \lim_{p \to 0} \frac{\mathbb{P}\left(\bigcup_{i=1}^{d} X_i > VaR_i(x_i p)\right)}{p}. \tag{3.16}$$

Roughly speaking, when p is at a low level, the function approximates the ratio between the probability that there is at the minimum one bank in distress and the tail probability p used before. For more discussions regarding this function, see e.g. De Haan and Ferreira (2007) and Zhou (2009).

Following the above definitions, the three measures can be estimated on $\boldsymbol{X}$ for $p \to 0$ as

$$PAO_i = L_{\neq i}(1, \ldots, 1) + (1 - L(1, \ldots, 1)) \,, \tag{3.17}$$

$$SII_i = \sum_{i=1}^{d} (2 - L_{i,j}(1, 1)) \,, \tag{3.18}$$

$$VI_i = \frac{L_{\neq i}(1, \ldots, 1) + (1 - L(1, \ldots, 1))}{L_{\neq i}(1, \ldots, 1)} \,, \tag{3.19}$$

where $L_{\neq i}(1, \ldots, 1)$ models the tail dependence between all banks except i, and $L_{i,j}(1, 1)$ captures the tail dependence only between the losses of banks i and j, for $i, j = 1, \ldots, d$ where $i \neq j$.

4 Data

The purpose of this study is to provide new insights in the dependence structure between banks in times of financial distress. Although traditional literature mainly focuses on interbank loans to capture the relation between these institutions, they are merely available one to four times per year due to the latest accounting standards. However, since this study uses EVT to construct an artificial banking sector, we need high-frequency data to ensure that enough observations in the tails of the distributions are available. That is why we consider two data sets. The first focuses on stock returns of individual banks and is used to compute the causal order and ML coefficient matrix of each bank in the system. The second data set consists of accounting data to relate the results, obtained from the first set, to the financial size of each bank.

To this end, we adopt a data set of daily U.S. equity returns to construct an artificial banking sector. In the spirit of Zhou (2009), the data set consists of thirty banks that are active on the NYSE during the period January 1, 1990 to December 31, 2014. Excluding non-trading days the sample consist of 6,523 returns for each bank. Returns are constructed by applying a log transformation on the return index and taking first differences. An important drawback is that

Table 1: Summary statistics for daily equity returns.
This table reports summary statistics for daily stock returns over the sample period January 2, 1990 to December 31, 2014. Reported are the mean, standard deviation (Std. dev.), minimum (Min.), maximum (Max.), skewness (Skew.), kurtosis (Kurt.) and the p-value of the Jarque-Bera (JB) test-statistic for normality of the data, respectively. Daily stock return data is based on data from Datastream. There are 6,522 observations and 30 banks included in the analysis. All values except the skewness and kurtosis are in percentages. The list consists of all banks that are preliminarily traded on the NYSE during the sample period. Further information regarding the bank names and historical context is given in Table D.1 in Appendix D.

Bank	Mean	Std. dev.	Min.	Max.	Skew.	Kurt.	JB
AB	0.056	2.224	−20.637	21.352	−0.214	11.922	0.000
ASB	0.030	2.070	−18.999	19.354	−0.131	14.020	0.000
BAC	0.018	2.714	−34.206	30.210	−0.336	30.221	0.000
BEN	0.059	2.236	−16.577	14.941	0.032	8.415	0.000
BK	0.042	2.342	−31.687	22.159	0.024	18.114	0.000
BOH	0.038	1.764	−25.508	12.946	−0.606	18.943	0.000
BXS	0.036	2.202	−17.575	19.711	0.055	10.641	0.000
CBU	0.051	2.113	−14.221	16.315	0.395	9.201	0.000
CFR	0.060	1.969	−21.457	19.782	0.351	14.011	0.000
CMA	0.035	2.165	−22.694	18.805	−0.190	16.713	0.000
CPF	−0.018	3.304	−43.570	32.312	−0.251	21.749	0.000
EV	0.069	2.379	−19.835	22.363	0.327	11.597	0.000
FHN	0.033	2.395	−44.114	25.545	−1.081	40.060	0.000
FNB	0.033	2.533	−25.533	19.567	−0.187	13.119	0.000
JEF	0.050	2.012	−23.233	20.764	−0.167	19.630	0.000
JPM	0.040	2.456	−23.228	22.392	0.248	14.041	0.000
KEY	0.021	2.562	−40.547	43.342	−0.463	46.117	0.000
LM	0.052	2.506	−28.438	26.509	−0.305	16.032	0.000
MTB	0.053	1.706	−16.972	19.110	0.249	17.774	0.000
PNC	0.036	2.248	−53.436	31.547	−1.230	66.805	0.000
RF	0.019	2.738	−52.885	39.481	−0.621	54.688	0.000
RJF	0.069	2.485	−26.118	22.021	0.184	12.675	0.000
SCHW	0.074	2.934	−21.123	23.222	0.302	7.170	0.000
SF	0.058	2.342	−27.112	32.439	0.534	15.594	0.000
SFE	0.026	3.944	−29.728	34.347	0.148	10.054	0.000
SNV	0.024	2.693	−30.069	24.858	−0.129	18.174	0.000
TFC	0.040	2.053	−26.608	21.198	0.129	19.548	0.000
USB	0.057	2.106	−20.047	25.764	0.176	19.426	0.000
WBS	0.041	2.541	−23.511	31.031	0.035	19.461	0.000
WFC	0.056	2.276	−27.210	28.341	0.743	27.865	0.000

they do not contain information about the size of the individual banks. Accordingly, we consider yearly assets, equity, and debt of the individuals banks over the sample period. All data are taken from Datastream.

Table 1 presents summary statistics for the daily equity returns. The sample distributions of the equity returns are non-symmetric around the mean, as the minimum returns are higher

in magnitude than the maximum returns. This suggests that the equity returns are non-normal, which is a well-known phenomenon in financial economics since the seminal paper of Mandelbrot (1963). The Jarcque-Bera test confirms this, since the null hypothesis of a normal distribution is rejected for all banks[3]. The main contributor to the non-normality of the distributions is the kurtosis, where a relatively high kurtosis implies that there are numerous observations outside the region of the peak of the sample distributions. In fact, all sample distributions are leptokurtic, where it can reach a kurtosis of more than 66. The contribution of the non-zero skewness is also significant, as demonstrated in the time series of daily returns in Figure D.2.

However, for the purpose of this research we are interested in the left tail of the sample distributions, which corresponds to the losses of each bank. Table 1 indicates that the skewness of each distribution is around zero or negative, suggesting that indeed the losses cause the tails to be heavy. Table D.2 in Appendix D provides further insights into the left tail of the distribution. To get an idea about the magnitude of the tails, the tail coefficient α is estimated, which is the reciprocal of the shape parameter ξ in the generalized Pareto distribution. These tails are typically gauged by means of the estimator proposed by Hill (1975), which heavily depends on the number of higher order extremes k that enter the estimation. Finding an optimal value for this threshold parameter is more an art than a science, where a commonly used heuristic plots the tail estimator as a function of k and selects the tail parameter in a region where $\hat{\xi}$ is stable[4]. These so-called Hill plots can be found in Figure D.3.

In addition to this heuristic, we formally test whether the tails are heavy by estimating the tail indexes based on the modified Hill-estimator developed by Huisman, Koedijk, Kool, and Palm (2001). This estimator is a weighted average of Hill estimators with weights derived from least squares estimation[5]. For the sake of hypothesis testing, a distribution is considered to have a fat tail if the hypothesis $\xi = 0$ is rejected in favor of $\xi > 0$. Table D.3 in Appendix D contains these estimates. From this table it can be concluded that all sample distributions are heavy-tailed, with a tail index around 3, which is in line with the evidence presented in financial literature that bank equity returns are non-normal and heavy-tailed (see e.g. Jansen and De Vries (1991), Gropp and Moerman (2004), and Hartmann et al. (2005)).

In terms of size, Table 2 presents summary statistics for the yearly balance sheet data. This table clearly shows the disparity between bank size, where the smallest bank has assets worth around 0.165 million USD on average, while the largest bank has more than 1,113 million USD.

[3]The Jarcque-Bera test considers whether observations have the skewness and kurtosis matching a normal distribution.

[4]As mentioned by Hill (1975), choosing an optimal k is a trade-off between bias and variance. When k is large, too many observations are used that are not in the tail, whereas a small threshold results in a high variance.

[5]This modified estimator is known for its unbiasedness and it outperforms alternative methods when used in the context of Value-at-Risk (see e.g. Brooks, Clare, Dalle Molle, and Persand (2005)).

Table 2: Summary statistics for yearly accounting data.
This table reports summary statistics for yearly assets, debts, and equity over the sample period January 2, 1990 to December 31, 2014. Reported are the mean and standard deviation (Std. dev.). All values are in millions of U.S dollars. Accounting data is based on data from Datastream. There 30 banks included in the analysis that are preliminarily traded on the NYSE during the sample period. Further information regarding the bank names and historical context is given Table D.1 in Appendix D.

	Total assets		*Total debt*		*Total equity*	
	Mean	Std. dev.	Mean	Std. dev.	Mean	Std. dev.
AB	1.174	0.503	0.044	0.089	1.019	0.615
ASB	14.524	8.519	2.844	1.940	1.456	1.005
BAC	1018.952	814.266	300.080	259.765	90.419	81.599
BEN	6.746	4.931	0.876	0.771	4.571	3.402
BK	139.778	115.923	13.966	9.224	14.259	12.814
BOH	12.356	1.850	2.269	1.294	0.954	0.185
BXS	8.476	4.644	0.603	0.554	0.786	0.485
CBU	3.441	2.316	0.443	0.340	0.364	0.299
CFR	10.949	7.282	0.658	0.435	1.043	0.829
CMA	46.570	16.020	7.108	3.626	4.190	1.917
CPF	2.993	1.740	0.323	0.326	0.296	0.242
EV	0.800	0.584	0.246	0.289	0.319	0.180
FHN	21.226	9.245	4.999	3.718	1.569	0.712
FNB	5.774	4.119	0.764	0.643	0.581	0.527
JEF	8.322	12.218	1.983	3.699	3.153	2.925
JPM	1063.896	869.466	271.437	225.625	79.981	72.387
KEY	79.442	18.191	16.463	7.804	6.573	2.250
LM	5.130	3.548	0.850	0.838	2.438	2.502
MTB	41.928	28.813	6.462	4.646	4.317	3.449
PNC	135.829	104.176	24.601	14.030	13.132	12.244
RF	68.897	52.804	9.270	8.522	7.690	6.769
RJF	9.306	7.822	0.718	0.968	1.260	1.169
SCHW	49.164	44.678	1.011	0.619	3.777	3.085
SF	1.849	2.741	0.229	0.234	0.462	0.684
SFE	0.630	0.381	0.169	0.081	0.250	0.179
SNV	18.632	10.718	1.738	1.176	1.749	1.058
TFC	85.628	66.579	15.448	10.622	8.480	7.144
USB	168.717	126.276	35.618	26.057	15.465	12.063
WBS	11.856	7.140	2.490	1.589	1.035	0.737
WFC	556.583	559.896	104.550	96.420	49.711	53.115

In terms of total assets, the list of largest banks includes JP Morgan, Bank of America, and Wells Fargo & Co. Their hegemony is reflected even further in the value of the total debt and equity, where the gap between the small and large banks increases. As noted by Zhou (2009), we lower the selection bias of using active banks during the sample period by including both small and large banks. This allows to construct a diverse banking system, where the relationship between banks can be related to their relative size.

5 Estimation procedure

This section discusses the estimation procedure for both max-linear models and systemic importance measures. First, Section 5.1 explains the required data transformation and estimation of the squared scalings for the recursive ML model. Subsequently, Section 5.2 shows how to estimate the L-function for the systemic importance measures.

5.1 Squared scalings

In Sections 3.3 and 3.4 we have established several relations to identify the ML coefficients through the squared scalings. The question remains how to estimate these scalings. As mentioned in Section 4, we consider daily equity returns of thirty banks, where the sample size is equal to 6,522. This is mathematically denoted as X_{lu}, for $l = 1, \dots, 6{,}522$ and $u = 1, \dots, 30$. To prepare these returns for the analysis, we must take two steps. First, since we consider downside risk, only negative returns should be taken into account. This is denoted as $X^+_{lu} = \max\{-X_{lu}, 0\}$. Second, the underlying distribution of each individual series must be Fréchet(2), which follows from the assumptions made in Section 3.3. That is why we employ the following probability integral transform on the returns

$$X^*_{lu} := \left[-\log\left(\frac{1}{n+1} \sum_{i=1}^{n} \mathbb{1}\{X^+_{iu} \leq X^+_{lu}\} \right) \right]^{-1/2}, \tag{5.1}$$

where $u \in V$ and $l = 1, \dots, 6{,}522$.

Next, the TPDM can be estimated. One important notion is that this matrix is symmetric positive semi-definite, such that either Singular Value Decomposition (SVD) or the Cholesky decomposition could be used to study the behaviour of the principal components. Both approaches have been studied by Cooley and Thibaud (2019). This paper restricts itself to estimating the squared scalings through the discrete spectral measure $S_{\boldsymbol{X}}(\cdot)$ as defined in (3.6). Klüppelberg and Krali (2021) show that the non-parametric estimator of these scalings is given by

$$\hat{\sigma}^2_{M_{\boldsymbol{h}}} = \frac{d}{N_n} \sum_{i=1}^{n} \bigvee_{u \in \boldsymbol{h}} \omega^2_{iu} \mathbb{1}\{R_i > x\}\,. \tag{5.2}$$

where $R_i = \|\boldsymbol{X}_i\|_2$, $\omega_{iu} = \frac{X_{iu}}{R_i}$, and $N_n = \sum_{i=1}^{n} \mathbb{1}\{R_i > \bar{R}\}$. Here, $\bar{R}$ is a threshold radius based on a certain k, where $1 \leq k \leq n$. In an initial setting, we choose $k = \sqrt{n}$, where its validity is reviewed in Section 7.3. A full derivation of the estimator is given in Section A.2 in Appendix A.

Consecutively, Algorithm C.1 and C.2 are run using the above estimator to obtain the initial vertices and their descendants in the DAG $\mathcal{D}$, respectively. To account for estimation errors,

three bounds z_j, for $j = 1, 2, 3$, are introduced, which are set to 0.1, 0.05 and 0.1, respectively. Algorithm C.1 calculates the difference between the two terms in equation (3.8) for each bank. If the difference is small (based on error bounds z_1 and z_2), we say that this particular vertex is a root vertex. In a similar fashion Algorithm C.2 recursively determines the order of the remaining vertices, by estimating the difference in equation (3.11). Identical to Klüppelberg and Krali (2021), the scalar a in these two representations is set equal to $\sqrt{2}$. Once the causal order is determined and squared scalings are estimated, the ML coefficients can be obtained using representation (3.7). Lastly, the in-degree, out-degree and betweenness centrality of each vertex in the system can be calculated using the aforementioned results.

5.2 L-function

To estimate the L-function, as presented in (3.16), this paper makes use of the non-parametric estimator $\hat{L}(\cdot)$, which is based on the Peaks over Threshold (PoT) approach. It considers observations that exceed a certain threshold, after which these excesses are to be modeled. Concretely, define the sequence $k := k(n)$, such that when the sample size $n \to \infty$, it holds that the number of extremes $k(n) \to \infty$ and the tail-fraction $k/n \to 0$. In that case, we can substitute the probability level for the tail-fraction and use the empirical distribution function of $\boldsymbol{X}$. Let the order statistics of $\boldsymbol{X}$ be denoted as $X_{i,1} \leq \cdots \leq X_{i,n}$, such that we can estimate the L-function as

$$\hat{L}(x_1, \ldots, x_d) = \frac{1}{k} \sum_{s=1}^{n} \mathbb{1}\{\exists 1 \leq i \leq d : X_{is} > X_{i,n-\lfloor kx_i \rfloor}\}\,. \tag{5.3}$$

Although the PoT approach provides the non-parametric estimator $\hat{L}(x_1, \ldots, x_d)$, its effectiveness rests on the selected hyper-parameter k. In fact, the threshold selection has a vast impact on the estimation of this parameter and is a trade-off between its variance and bias. For instance, when the threshold is set too high there are only a few observations considered; causing a high variance of the parameter. Conversely, a low threshold causes too many observations from the center of the distribution to be included, which results in biased estimates. That is why, similar to Zhou (2009), k is chosen in such a way that it corresponds to tail probability levels 1%, 2.5% and 5%.

6 Empirical results

6.1 Underlying banking structure

Table 3 presents the causal order and centrality measures for each bank. As expected, there exists an inverse relationship between the order and out-degree of the banks due to the ayclic nature of the graph. Intuitively, more influential banks, which cause most of the systemic risk, have a higher spread rate than other banks. It seems that the influential banks are in fact large banks in terms of size, since they achieve a higher order than smaller banks. To formally test this observation, three correlation measures are calculated to capture the relation between size, in- and out-degree, and the causal order. The correlation coefficients are estimated by means of a moving window analysis, where the window size is eight years to ensure that enough observations are included in the estimation procedure. Table 4 contains these values and evidently shows that indeed larger banks have a higher causal order. At the same time, they have a lower in-degree; meaning that less risk comes to them from other banks.

The ML coefficients can be used to exactly determine which banks cause the incoming risk flow to large banks. Overall, most of the incoming risk is coming from other large banks, while small banks have only a small contribution in the total incoming risk. This phenomenon is described in other literature as well. For example, Hartmann et al. (2005) finds that the largest institutions within one country are not always interlinked, because the demand for credit between these institutions is often low. Elsinger, Lehar, and Summer (2006) demonstrates that small banks are more dependent on large banks than the other way around due to outstanding credit. Similarly, we observe that small banks spread less risk to other banks, while they absorb more. This fits with the aforementioned phenomenon that smaller banks take more credit from other banks.

One interesting observation is that average sized banks tend to have betweenness values in the center of the distribution. According to Table 3, these banks often have more balanced flow between the number of incoming and outgoing connections. This makes them important in the eyes of policy makers, as they facilitate the flow of risk from one bank to another. By protecting these banks during a crisis, the domino effect will be put to hold as a chunk of the flow will be stopped towards the remaining parts of the system.

6.2 Systematic importance measure

To relate the results of the ML model to existing financial measures, we estimate the systematic importance measure of each bank by means of equations (3.17)-(3.19). Table 5 shows that there

Table 3: Performance measures for graphical models.
This table reports the performance measures for the graphical models over the sample period January 2, 1990 to December 31, 2014. Reported are the causal order (Rank), bank ticker (Bank), in-degree of the nodes (In-degree), out-degree of the nodes (Out-degree), and betweenness centrality measure (Betweenness), respectively. There are 30 banks included in the analysis that are preliminary traded on the NYSE during the sample period. Further information regarding the bank names and historical context is given Table D.1 in Appendix D.

Rank	Bank	In-degree	Out-degree	Betweenness
1	TFC	0	29	0.000
2	SCHW	1	28	0.000
3	RJF	2	25	0.000
4	JPM	3	21	0.250
5	CMA	4	21	0.341
6	BK	4	16	1.183
7	AB	4	10	14.324
8	BAC	5	19	2.819
9	JEF	7	10	2.310
10	USB	8	12	0.000
11	SF	7	13	1.584
12	PNC	9	3	10.969
13	WFC	11	14	15.612
14	RF	9	7	4.062
15	SNV	8	15	4.591
16	WBS	9	5	19.489
17	FHN	12	0	3.488
18	MTB	10	11	0.000
19	LM	12	8	2.291
20	EV	13	9	8.931
21	KEY	15	1	1.460
22	ASB	12	0	0.000
23	SFE	12	1	8.679
24	FNB	16	6	4.583
25	CBU	16	0	1.500
26	BOH	14	4	5.333
27	BEN	17	0	0.000
28	CFR	17	1	7.200
29	BXS	16	1	0.000
30	CPF	16	0	0.000

is less variation between banks when using a high p-value. This is due to how accurate the measures are calculated. When using a higher p-value, more observations outside the tail region are included, which leads to less noise in the estimation. Looking at the magnitude of the values, we find that both CMA and WFC score high SII and PAO levels for all p-values. This is unsurprising, since they belong to the upper quantile of the size distribution. However, it is interesting that WFC also scores high for VI. A possible explanation can be found in Table 2,

Table 4: Correlation between size and centrality.
This table reports correlation values between size and centrality over the sample period January 2, 1990 to December 31, 2014. Size corresponds to total assets, debt and equity, whereas centrality entails the in- and out-degree and the causal order (Rank). Accounting data is based on data from Datastream. The centrality measures are obtained by employing Algorithm C.1 and C.2. Reported are the Pearson, Spearman, and Kendall correlation. Significance at the 10%-, 5%-, and 1%-level are indicated by *, **, and ***, respectively.

	In-degree	Out-degree	Rank
Panel A: Pearson			
Total assets	−0.075***	0.058***	0.088***
Total debt	−0.081***	0.057***	0.087***
Total equity	−0.077***	0.060***	0.091***
Panel B: Spearman			
Total assets	−0.090***	0.130***	0.128***
Total debt	−0.114***	0.144***	0.148***
Total equity	−0.084***	0.124***	0.122***
Panel C: Kendall			
Total assets	−0.064***	0.090***	0.088***
Total debt	−0.081***	0.100***	0.087***
Total equity	−0.060***	0.060***	0.091***

which shows that WFC belongs in the top-three highest debts. A higher debt signals that this bank is more dependent on other banks, which coincides with the definition of the VI.

When focusing on $p = 5\%$, we find a lot of diversity between the different measures. Specifically, RF, KEY and WFC rank highest in SII, PAO and VI, respectively. The former two banks are now included in this list, because we consider more observations outside the tail region. This ensures that the level of distress is set lower and more observations of average sized banks are taken into account as well.

As before, three correlation coefficients are calculated between systematic importance and centrality measures. Table 6 contains these coefficients for $p = 0.05$. First, the causal order of the banking system is considered. From Table 6 it is clear that there exists a positive relation between the causal order and the probability that one banks causes another to fall; that is, the PAO. This is expected from the definition of the causal order. At the same time, there is a weak relation between the degree in which banks cause the spread of risk and the chance of being in distress due to other banks that are in distress. That is because the index takes into account effects from both large and small banks. However, as we have discussed before, the effects from small to large banks are reducible and the effects from large to large is overall small.

One should notice the difference in significance between the correlation coefficients. Evi-

Table 5: Systemic measures for US banks.
This table reports the systemic measures over the sample period January 2, 1990 to December 31, 2014. These measures are calculated for tail probability levels 1%, 2.5% and 5%. SII is the systemic importance index, defined as the number of expected bank failures given a particular bank fails; see (2). PAO is the probability of having at least one extra bank failure when a particular bank fails, defined in (1). VI is the vulnerability index, defined as the probability of failure given there exists at least another bank failure in the system; see (3). There are 6,523 observations and 30 banks included in the analysis. All values except the SII are in percentages. Further information regarding the bank names and historical context is given in Table D.1 in Appendix D.

	p = 0.010			*p = 0.025*			*p = 0.050*		
	SII	PAO	VI	SII	PAO	VI	SII	PAO	VI
AB	9.985	73.846	7.028	9.276	74.847	7.974	9.831	84.356	10.296
ASB	10.508	83.077	7.837	11.215	86.503	9.103	11.104	85.890	10.463
BAC	12.200	90.769	8.501	11.890	87.730	9.220	12.298	93.558	11.292
BEN	9.800	81.538	7.703	10.975	85.890	9.044	11.515	88.957	10.797
BK	10.985	90.769	8.501	10.411	87.730	9.220	11.552	92.331	11.161
BOH	9.754	76.923	7.299	11.018	85.890	9.044	11.745	92.025	11.128
BXS	8.200	52.308	5.082	8.607	65.031	7.001	9.110	78.221	9.619
CBU	6.677	44.615	4.367	7.994	66.258	7.124	8.933	79.448	9.755
CFR	8.292	64.615	6.204	8.957	77.301	8.214	10.245	87.730	10.664
CMA	12.538	92.308	8.633	12.356	94.479	9.859	12.840	93.558	11.292
CPF	7.892	63.077	6.065	8.914	66.258	7.124	8.620	73.313	9.070
EV	10.215	73.846	7.028	10.344	75.460	8.034	9.991	81.288	9.959
FHN	10.431	80.000	7.569	11.485	90.184	9.453	11.893	91.104	11.029
FNB	7.923	41.538	4.079	8.123	56.442	6.133	8.727	70.245	8.724
JEF	10.862	83.077	7.837	10.834	80.982	8.571	10.813	83.742	10.229
JPM	11.169	87.692	8.237	10.816	88.344	9.278	11.933	95.399	11.489
KEY	12.523	90.769	8.501	12.712	93.865	9.801	12.862	96.319	11.587
LM	10.815	84.615	7.971	10.902	82.822	8.749	11.015	88.037	10.697
MTB	11.892	90.769	8.501	12.202	90.798	9.512	12.294	92.331	11.161
PNC	11.385	87.692	8.237	11.620	88.344	9.278	12.077	91.104	11.029
RF	11.908	92.308	8.633	12.436	93.252	9.744	12.914	92.945	11.226
RJF	10.538	73.846	7.028	10.104	85.276	8.985	10.923	87.117	10.597
SCHW	5.846	55.385	5.365	7.215	74.233	7.914	9.175	88.957	10.797
SF	6.862	58.462	5.646	8.325	68.098	7.307	8.933	73.006	9.036
SFE	4.985	49.231	4.798	6.939	65.644	7.063	7.460	71.779	8.897
SNV	9.892	84.615	7.971	10.748	84.663	8.926	11.279	86.503	10.530
TFC	10.615	86.154	8.104	11.595	86.503	9.103	12.160	91.411	11.062
USB	10.938	86.154	8.104	11.147	85.276	8.985	11.417	91.411	11.062
WBS	10.800	80.000	7.569	10.767	83.436	8.808	11.049	85.276	10.396
WFC	12.185	95.385	8.895	11.767	88.344	9.278	12.331	93.865	11.325

dently, the Pearson coefficients in Panel A of Table 6 are weakly significant to insignificant, while the Spearman and Kendall coefficients in Panels B and C, respectively, are almost all highly significant. The reason for this can be found in the underlying calculation of the former measure. Specifically, the Pearson correlation assumes a linear relation whereas the Spearman

Table 6: Correlation between systemic importance and centrality.
This table reports correlation values between systemic importance measures and centrality over the sample period January 2, 1990 to December 31, 2014. Reported are both the systemic importance measures PAO, VI and SII assets, debt and equity, and centrality indicators in- and out-degree and the causal order (Rank). Accounting data is based on data from Datastream. The centrality measures are obtained by employing Algorithm C.1 and C.2. Reported are the Pearson, Spearman, and Kendall correlation. Significance at the 10%-, 5%-, and 1%-level are indicated by *, **, and ***, respectively.

	In-degree	Out-degree	Rank
Panel A: Pearson			
PAO	0.005	0.022*	0.039***
VI	−0.007	0.004	0.014
SII	−0.009	0.013	0.024*
Panel B: Spearman			
PAO	−0.064***	0.096***	0.100***
VI	−0.022*	−0.036***	0.024*
SII	−0.020	0.048***	0.032**
Panel C: Kendall			
PAO	−0.049***	0.069***	0.074***
VI	−0.016*	−0.025***	0.017**
SII	−0.016*	0.033***	0.023***

correlation converts the levels to ranks and uses those to determine the relation. Kendall's correlation is more robust, as it considers the probabilities of observing the concordant and discordant pairs.

In sum, we observe that the methods of Klüppelberg and Krali (2021) yield similar outcomes as existing literature but from another perspective. Specifically, we find that small banks suffer from contagion risk which originates from large banks. Combining the constructed graph with topological measures, such as vertex degrees, a more in-depth analysis is conducted since they can be related to existing systemic importance measures.

7 Robustness analysis

This section verifies the robustness of the results presented in Section 6. The consequences of changes in the data frequency are evaluated in Section 7.1. Subsequently, excess returns are constructed and a similar procedure is conducted in Section 7.2. The effects of the hyperparameters are evaluated in Section 7.3.

Table 7: Performance measures using weekly equity returns.
This table reports the performance measures for the graphical models over the sample period January 2, 1990 to December 31, 2014 using weekly returns. Reported are the causal order (Rank), bank ticker (Bank), in-degree of the nodes (In-degree), out-degree of the nodes (Out-degree), and betweenness centrality measure (Betweenness), respectively. There are 30 banks included in the analysis that are preliminary traded on the NYSE during the sample period. Further information regarding the bank names and historical context is given Table D.1 in Appendix D.

Rank	Bank	In-degree	Out-degree	Betweenness
1	BK	0	29	0.000
2	SCHW	1	24	0.000
3	SNV	2	8	0.056
4	SF	2	23	0.818
5	RJF	3	2	0.000
6	AB	3	22	7.468
7	KEY	4	5	0.686
8	JPM	3	16	0.431
9	FNB	5	13	6.851
10	EV	5	19	2.369
11	CPF	5	12	1.483
12	CMA	8	13	5.473
13	CFR	6	12	5.000
14	BEN	8	9	12.405
15	BAC	8	7	4.505
16	RF	9	9	5.619
17	CBU	12	9	8.037
18	TFC	13	9	16.592
19	WFC	12	9	6.913
20	BOH	12	6	3.773
21	WBS	13	6	4.723
22	USB	13	7	3.320
23	PNC	14	5	8.204
24	BXS	14	5	1.931
25	JEF	17	4	1.197
26	SFE	21	3	1.325
27	ASB	22	2	0.938
28	FHN	14	0	0.000
29	LM	22	1	0.882
30	MTB	18	0	0.000

7.1 Low-frequency data

So far, we have considered daily data to model the dependence structure between banks. The advantage of having high-frequency data is that it allows us to perform an in-depth analysis of the tails. At the same time, they might suffer from the interdependent problem on the time dimension (Diebold, Schuermann, & Stroughair, 1998). To reduce these effects, we consider lower-frequency data such as weekly equity returns. Although monthly data are used more often in financial literature, it does not suit our methodology well. This is because of the significant reduction in observations above our chosen thresholds. That is why weekly data are used, which still given some insight in the effects of low frequency.

The results are captured in Table 7. The causal order for the top-10 banks is similar to the one obtained in Section 6.1. However, smaller banks have shuffled significantly in this ranking. This could be due to the cumulative nature of weekly compared to daily returns. Noteworthily, the betweenness centrality of the middle sized banks' are less volatile, implying that more banks are likely to spread risk to the small banks. Tables E.1 and E.2 in Appendix E further shows the impact of weekly equity returns on the correlation between the graph and size, and the graph and systemic importance measures, respectively. Overall, the sign of the dependence between the measures are similar to those in Section 6, but the magnitude is smaller. This could be due to the lower frequency of the data, which ensures that negative effects are often compensated by accumulated positive effects.

7.2 Excess returns

So far, we have considered equity returns to model the dependence structure between banks. Although this is a common approach in existing literature, it does not take into account a benchmark which is of interest to policy makers and investors. For example, European Central Bank uses excess returns to model their relationship to the size of a bank (Castrén, Fitzpatrick, & Sydow, 2006). As such, another approach is to consider excess returns, which are constructed deducting the risk-free rate from the returns as described in Section 4. The 3-month LIBOR rate is taken as a proxy for the risk-free rate and is obtained from the Federal Reserve Bank of St. Louis and spans the same time period as the daily equity returns[6].

The performance of the recursive ML model optimized with daily excess equity returns is displayed in Table 8. It seems that the causal order of the banks remains similar to the one presented in Section 6. This observation is confirmed by the correlation measures in Table E.3 in Appendix E. However, there is one notable difference: large banks remain high in the ranking,

[6] See: `https://fred.stlouisfed.org`.

Table 8: Performance measures using excess returns.
This table reports the performance measures for the graphical models over the sample period January 2, 1990 to December 31, 2014. Reported are the causal order (Rank), bank ticker (Bank), in-degree of the nodes (In-degree), out-degree of the nodes (Out-degree), and betweenness centrality measure (Betweenness), respectively. There are 30 banks included in the analysis that are preliminary traded on the NYSE during the sample period. Excess returns are constructed by subtracting 1-month LIBOR rates from the daily equity returns in Section 4. Further information regarding the bank names and historical context is given Table D.1 in Appendix D.

Rank	Bank	In-degree	Out-degree	Betweenness
1	SCHW	0	29	0.000
2	RJF	1	26	0.033
3	PNC	2	16	0.396
4	CMA	2	23	0.396
5	BK	3	24	1.630
6	BAC	4	0	0.000
7	AB	4	11	1.694
8	KEY	4	18	2.220
9	JPM	4	20	0.407
10	MTB	8	9	3.242
11	FHN	7	12	2.928
12	WBS	9	1	0.033
13	TFC	8	13	4.936
14	SNV	10	12	6.878
15	BEN	9	14	8.861
16	CPF	12	0	0.000
17	EV	10	11	5.733
18	USB	9	3	1.111
19	BOH	10	8	3.191
20	WFC	12	3	1.897
21	JEF	14	9	9.025
22	CBU	12	1	0.286
23	BXS	14	7	10.342
24	CFR	13	5	0.799
25	LM	16	5	2.334
26	FNB	17	0	0.786
27	SF	18	0	0.000
28	SFE	14	1	0.188
29	ASB	18	1	0.388
30	RF	17	0	0.000

whilst the lowest banks shuffled. Hence, small banks are affected the most in their structure when taking the risk-free rate into account. This effect is also found in Table E.3, where most coefficients are smaller in magnitude than before. A possible explanation for this is that the daily returns for small banks are generally small, such that subtracting the risk-free rate can have a large impact on the estimation results. Interestingly, the relation between systemic importance and centrality becomes stronger as shown in Table E.4.

7.3 Parameter tuning

A last crucial element of the recursive ML model is the hyper-parameter set. Tuning the parameters often causes either more or less observations to be included, which as a result changes the overall conclusion of our research. In general, there are three types of hyper-parameters that we consider: the error bounds z_i, for $i = 1, 2, 3$, that decide the order of the vertices in the graph, a which is the constant in equation 3.8, and the threshold radial component $R^{(k)}$. The first two types are used in Algorithms C.1 and C.2, whereas the latter type determines how many observations are included in the sample. Theoretically, when the errors bounds z_1 and z_2 are large, many vertices are considered to be potential candidates in the root of the graph. Conversely, small error bounds ensure a limited group of initial vertices. It is, therefore, important to find a balance between these two cases. As before, let $a = \sqrt{2}$ and consider the possible values $z_i \in \{0.01, 0.05, 0.1, 0.5\}$, for $i = 1, 2$.

Unsurprisingly, we see that tight error bounds lead to similar results as before, whereas large bounds cause the causal order to be equal to the order in which the banks are given to the code. Similar results hold for the scalar a when it can take on values from the set $\{1.01, 1.5, 2, 4\}$. Hence, the values suggested by Klüppelberg and Krali (2021) are most plausible in the sense that they allow sufficient vertices in the root of the graph, while at the same time limiting the volatility between the squared scalings.

Finally, several k-th upper statistics are considered to estimate the radial threshold. Similar to the systemic importance measures, k is chosen such that the tail probabilities are 1.0%, 2.5% and 5.0%. Evidently, we find that for high tail probabilities the results stay similar to those presented in Section 6.1. However, when selecting high k values the results change drastically. This is due to sharp decrease in the number of observations that are included in the sample. Now middle sized banks are dominant in the top of the causal order, while large banks have average performance. One possible explanation for this is that the sample for middle sized banks contain larger losses than those of large banks. Consequently, the losses for middle sized banks dominate in the sample which is used to determine the causal order.

8 Conclusion

This paper studies how the latest insight in recursive ML models can discover the hidden structure in a banking system. The focus is on measuring contagion risk, such that extreme spillovers among banks can be captured. The global financial crisis of 2007–2008 has demonstrated the need for an improved understanding of these measures. Particularly, the interconnectedness of companies during times of financial distress thwarts the construction of suitable risk measures. That is why the empirical application uses daily equity returns and yearly balance-sheet data of U.S. banks listed in the NYSE in the period from 1990 to 2015 to model their dependence structure. Specifically, the daily returns are used to obtain the causal order of, and dependence structure between, each bank in the system, whereas the accounting data relates the outcome of each bank to its relative financial size.

Our empirical analysis show the relations between U.S. banks and clearly flag flows of potential risk spillovers. In particular, large banks tend to influence most of the banks in the banking system through intermediary, average sized banks. Consequently, the contagion risk of small banks is relatively high, causing them to be most vulnerable to the validity of system. Although most results are in line with existing literature, we find the probability that a bank defaults due to the default of other banks is negatively correlated with size, which is in contrast with the results of Zhou (2009). The reason for this could be in the underlying assumptions of the ML model, such as the acyclic nature of the imposed graph. The findings become more modest when considering a wide range of robustness checks. Nevertheless, they provide a similar interpretation as before.

Our research has considerable social implications. Specifically, traditional systemic importance measures can be seen as the first indicators of an early warning system, that signals the stress levels of a vital bank for the system. Afterwards, the recursive ML model can be applied on this system to find the explicit dependence structure between banks and pinpoint the bottlenecks in the system. These bottlenecks can ensure that downward risk spreads fast across the system, so that their identification is crucial. Obviously, all of the aforementioned is based on accurate and concise market signals. Policy makers are obliged to set strict thresholds for these measures, after which the regulator can assess the situation in the banking system.

The methodology used in this paper has some limitations. For instance, the innovations vector is assumed to have a tail index $\alpha = 2$, which is often not found in empirical data. This is evidently present in the context of financial time series, where stock returns often display a tail index around 3. Therefore, future research may be dedicated to improving the method of

Klüppelberg and Krali (2021) by taking varying tail indices into account. Another limitation is that the methodology does not take into account the time dependence in the data when fitting the recursive ML model. Although this is preferred from a theoretical standpoint, doing so is not trivial in recursive ML models such that more research needs to be conducted in this field.

A final avenue that deserves attention in future studies lies in CDS spreads. Although equity returns are commonly used in modeling system risk (see, e.g., Zhou (2009), Hartmann et al. (2005), Castrén et al. (2006)), it is in fact the CDS market that leads the credit rating agencies and its returns are closely related to economic risk indicators (Hull, Predescu, & White, 2005). Moreover, Rodríguez-Moreno and Peña (2013) emphasize the explanatory power of CDS spreads, where systemic risk measures based on CDSs outperform measures using stock prices. Ideally, the higher liquidity of CDS enhance the ability of the recursive ML model to gauge the contagion risk in the US banking system, such that a concrete early-warning system can be designed.

References

Allen, F., & Babus, A. (2009). Networks in finance. *The network challenge: strategy, profit, and risk in an interlinked world*, *367*.

Allen, F., Babus, A., & Carletti, E. (2009). Financial crises: theory and evidence. *Annual Review of Financial Economics*, *1*(1), 97–116.

Allen, F., & Gale, D. (2000). Financial contagion. *Journal of Political Economy*, *108*(1), 1–33.

Boss, M., Elsinger, H., Summer, M., & Thurner, S. (2004). Network topology of the interbank market. *Quantitative Finance*, *4*(6), 677–684.

Brooks, C., Clare, A., Dalle Molle, J. W., & Persand, G. (2005). A comparison of extreme value theory approaches for determining value at risk. *Journal of Empirical Finance*, *12*(2), 339–352.

Buck, J., & Klüppelberg, C. (2020). Recursive max-linear models with propagating noise. *arXiv preprint arXiv:2003.00362*.

Castrén, O., Fitzpatrick, T., & Sydow, M. (2006). What drives eu banks' stock returns? bank-level evidence using the dynamic dividend-discount model.

Cooley, D., & Thibaud, E. (2019). Decompositions of dependence for high-dimensional extremes. *Biometrika*, *106*(3), 587–604.

Danielsson, J., Jorgensen, B. N., Mandira, S., Samorodnitsky, G., & De Vries, C. G. (2005). *Subadditivity re-examined: the case for value-at-risk* (Tech. Rep.). Cornell University Operations Research and Industrial Engineering.

Davis, R. A., & Resnick, S. I. (1989). Basic properties and prediction of max-arma processes. *Advances in applied probability*, 781–803.

De Bandt, O., & Hartmann, P. (2000). Systemic risk: a survey.

De Haan, L., & Ferreira, A. (2007). *Extreme value theory: an introduction*. Springer Science & Business Media.

De Jonghe, O. (2010). Back to the basics in banking? a micro-analysis of banking system stability. *Journal of financial intermediation*, *19*(3), 387–417.

Diebold, F. X., Schuermann, T., & Stroughair, J. D. (1998). Pitfalls and opportunities in the use of extreme value theory in risk management. In *Decision technologies for computational finance* (pp. 3–12). Springer.

Einmahl, J. H., Kiriliouk, A., & Segers, J. (2018). A continuous updating weighted least squares estimator of tail dependence in high dimensions. *Extremes*, *21*(2), 205–233.

Eisenberg, L., & Noe, T. H. (2001). Systemic risk in financial systems. *Management Science*, *47*(2), 236–249.

Elsinger, H., Lehar, A., & Summer, M. (2006). Risk assessment for banking systems. *Management science*, *52*(9), 1301–1314.

Engelke, S., & Hitz, A. S. (2018). Graphical models for extremes. *arXiv preprint arXiv:1812.01734*.

Engelke, S., & Ivanovs, J. (2020). Sparse structures for multivariate extremes. *arXiv preprint arXiv:2004.12182*.

Forbes, K. J., & Rigobon, R. (2002). No contagion, only interdependence: measuring stock market comovements. *The journal of Finance*, *57*(5), 2223–2261.

Freixas, X., Parigi, B. M., & Rochet, J.-C. (2000). Systemic risk, interbank relations, and liquidity provision by the central bank. *Journal of Money, Credit and Banking*, 611–638.

Furfine, C. H. (2003). Interbank exposures: Quantifying the risk of contagion. *Journal of Money, Credit and Banking*, 111–128.

Gai, P., & Kapadia, S. (2010). Contagion in financial networks. *Proceedings of the Royal Society A: Mathematical, Physical and Engineering Sciences*, *466*(2120), 2401–2423.

Georg, C.-P. (2013). The effect of the interbank network structure on contagion and common shocks. *Journal of Banking & Finance*, *37*(7), 2216–2228.

Gissibl, N., & Klüppelberg, C. (2018). Max-linear models on directed acyclic graphs. *Bernoulli*, *24*(4A), 2693–2720.

Gissibl, N., Klüppelberg, C., & Lauritzen, S. (2019). Identifiability and estimation of recursive max-linear models. *arXiv preprint arXiv:1901.03556*.

Gnecco, N., Meinshausen, N., Peters, J., & Engelke, S. (2019). Causal discovery in heavy-tailed models. *arXiv preprint arXiv:1908.05097*.

Gropp, R., & Moerman, G. (2004). Measurement of contagion in banks' equity prices. *Journal of International Money and Finance*, *23*(3), 405–459.

Hartmann, P., Straetmans, S., & De Vries, C. G. (2005). *Banking system stability: A cross-atlantic perspective* (Tech. Rep.). National Bureau of Economic Research.

Hill, B. M. (1975). A simple general approach to inference about the tail of a distribution. *The annals of statistics*, 1163–1174.

Huisman, R., Koedijk, K. G., Kool, C. J. M., & Palm, F. (2001). Tail-index estimates in small samples. *Journal of Business & Economic Statistics*, *19*(2), 208–216.

Hull, J. C., Predescu, M., & White, A. (2005). Bond prices, default probabilities and risk premiums. *Default Probabilities and Risk Premiums (March 9, 2005)*.

Jansen, D. W., & De Vries, C. G. (1991). On the frequency of large stock returns: Putting booms and busts into perspective. *The review of economics and statistics*, 18–24.

Klüppelberg, C., & Krali, M. (2021). Estimating an extreme bayesian network via scalings. *Journal of Multivariate Analysis*, *181*, 104672.

Larsson, M., & Resnick, S. I. (2012). Extremal dependence measure and extremogram: the regularly varying case. *Extremes*, *15*(2), 231–256.

Mandelbrot, B. (1963). New methods in statistical economics. *Journal of political economy*, *71*(5), 421–440.

Martinez-Jaramillo, S., Alexandrova-Kabadjova, B., Bravo-Benitez, B., & Solórzano-Margain, J. P. (2014). An empirical study of the mexican banking system's network and its implications for systemic risk. *Journal of Economic Dynamics and Control*, *40*, 242–265.

Nijskens, R., & Wagner, W. (2011). Credit risk transfer activities and systemic risk: How banks became less risky individually but posed greater risks to the financial system at the same time. *Journal of Banking & Finance*, *35*(6), 1391–1398.

Pearl, J. (2009). *Causality*. Cambridge university press.

Resnick, S. I. (2007). *Heavy-tail phenomena: probabilistic and statistical modeling*. Springer Science & Business Media.

Rodríguez-Moreno, M., & Peña, J. I. (2013). Systemic risk measures: The simpler the better? *Journal of Banking & Finance*, *37*(6), 1817–1831.

Segers, J. (2019). One-versus multi-component regular variation and extremes of markov trees. *arXiv preprint arXiv:1902.02226*.

Segoviano Basurto, M., & Goodhart, C. (2009). Banking stability measures. *IMF working papers*, 1–54.

Upper, C., & Worms, A. (2004). Estimating bilateral exposures in the german interbank market:

Is there a danger of contagion? *European Economic Review*, *48*(4), 827–849.

Valencia, F., Laeven, L., et al. (2008). *Systemic banking crises; a new database* (Tech. Rep.). International Monetary Fund.

Zhang, Z., & Smith, R. L. (2004). The behavior of multivariate maxima of moving maxima processes. *Journal of Applied Probability*, 1113–1123.

Zhou, C. (2009). Are banks too big to fail? Measuring systemic importance of financial institutions. *Measuring Systemic Importance of Financial Institutions (December 1, 2009)*.

A Mathematical notation and derivations

Table A.1: Variable descriptions.
This table provides descriptions and definitions of the variables used throughout the paper. Panel A concerns graphical variables, Panel B dependent variables, and Panel C control variables.

Variable name	Description
Panel A: Graphical notation	
$\mathcal{D}$	A directed acyclic graph that is defined on the random vector $\boldsymbol{X}$.
V	The set of vertices on the graph $\mathcal{D}$. These vertices consist of the d banks that are captured in the random vector $\boldsymbol{X}$.
E	The set of edges defined as $\{(v,u) : u \in V \text{ and } v \in \text{pa}(u)\}$.
$\text{pa}(u)$	The set of parents of vertex u, where a parent is the immediate predecessor of u.
$\text{an}(u)$	The set of ancestors of vertex u, where an ancestor is a predecessor which allows to end up at u through a directed path.
$\text{An}(u)$	The set of ancestors of vertex u including the vertex itself; that is $\text{An}(u) = \text{an}(u) \cup \{u\}$.
p_{vu}	One of the possible paths from vertex v to u. The length of the path is given by $\lvert p_{vu}\rvert = m$.
c_{uv}	The edge weight from vertex v to u, for which it must hold that $v \in \text{pa}(u)$.
$d_{vu}(p)$	The weight of a path p_{vu} from vertex v to u, which is defined as $c_{k_0,k_0}\prod_{l=0}^{m-1} c_{k_l,k_{l+1}}$.
ε_u	Independent and identically distributed innovations that capture omitted factors. Their distributions are assumed to be atom-free.
b_{uv}	The max-linear coefficient from the recursive ML model $X_u = \bigvee_{v\in\text{An}(u)} b_{uv}\varepsilon_u$. All coefficients are captured in the d-by-d square matrix B.
$S_{\boldsymbol{X}}(\cdot)$	The spectral measure defined on the Borel subsets of the unit hypersphere $\boldsymbol{\Theta}_{d-1} = \left\{\boldsymbol{\theta} \in \mathbb{R}^d : \lVert\boldsymbol{\theta}\rVert = 1\right\}$.
Panel B: Systemic measures importance	
$L(\boldsymbol{x})$	Function that characterizes the co-movement of extreme events between banks and is given by $L(\boldsymbol{x}) = \lim_{p\to 0}\frac{1}{p} \times \mathbb{P}\left(\bigcup_{i=1}^d X_i > VaR_i(x_i p)\right)$.
$\text{PAO}_i(p)$	The conditional probability that at least one bank fails, given that bank i fails, for $i = 1,\ldots,d$. The formula is given by $PAO_i(p) = \mathbb{P}\left(\{\exists j \neq i : X_j > VaR_j(p)\} \mid X_i > VaR_i(p)\right)$.
$\text{SII}_i(p)$	The expected number of banks that fail, given that bank i fails, for $i = 1,\ldots,d$. The formula is given by $SII_i(p) = \mathbb{E}\left(\sum_{j=1}^d \mathbb{1}_{X_j > VaR_j(p)} \mid X_i > VaR_i(p)\right)$.

VI_i	The conditional probability that bank i fails, given that at least one other bank fails, for $i = 1, \ldots, d$. The formula is given by $VI_i(p) = \mathbb{P}\left(X_i > VaR_i(p) \mid \{\exists j \neq i : X_j > VaR_j(p)\}\right)$.
Panel C: Centrality measures	
$\lambda_{wu}(v)$	The number of shortest paths that start at vertex w, go through vertex v and end at vertex u.
λ_{wu}	The total number of shortest paths from vertex w to u.

Table A.2: Operator descriptions.
This table provides descriptions and definitions of those operators used throughout the paper for which different definitions exist in the academic literature.

Operator	Description
$\bigvee$	The maximum over a set of realizations. For example, the notation $\bigvee_{i=1}^{k} c_i$ is equivalent to the maximum $\max\{c_i : 1 \leq i \leq k\}$.
$\odot$	The matrix product $\mathbb{R}_+^{m\times n} \times \mathbb{R}_+^{n\times p} \to \mathbb{R}_+^{m\times p}$, which is defined as $(F \odot G)_{ik} = \bigvee_{j=1}^{m} f_{ij} g_{jk}$ for $i = 1, \ldots, n$ and $k = 1, \ldots, m$.

A.1 Spectral measure

Consider a d-dimensional cone $\mathbb{C} = [0, \infty]^d \setminus \{\mathbf{0}\}$ on a Borel space and let ν be a non-zero Radon measure on $\mathbb{C}$[7]. Then a random vector $\boldsymbol{X}$ on $\mathbb{C}$ has multivariate regularly varying tails if there is a non-negative normalizing function $b(n)$ and Radon measure $\nu_{\boldsymbol{X}}$ on $\mathbb{C}$ such that

$$n\,\mathbb{P}\left(\frac{\boldsymbol{X}}{b(n)} \in \cdot\right) \xrightarrow{v} \nu_{\boldsymbol{X}}(\cdot)\,, \tag{A.1}$$

where $\xrightarrow{v}$ denotes vague convergence. Consequently, we write $\boldsymbol{X} \in \text{MRV}_{\alpha}^{d}$ with tail index $\alpha > 0$.

As $\nu_{\boldsymbol{X}}$ has several convenient scaling properties, it is appropriate to consider polar coordinates. Define $\boldsymbol{\Theta}_{d-1} := \left\{\boldsymbol{\theta} \in \mathbb{R}^d : \|\boldsymbol{\theta}\| = 1\right\}$ as the unit hypersphere and let the polar coordinate transformation $\psi : \mathbb{C} \to (0, \infty] \times \boldsymbol{\Theta}^{d-1}$ be defined as

$$\boldsymbol{x} \mapsto (R, \boldsymbol{\omega}) = \left(\|\boldsymbol{x}\|_2, \frac{\boldsymbol{x}}{\|\boldsymbol{x}\|_2}\right)\,. \tag{A.2}$$

According to Theorem 6.1 of Resnick (2007), the above transformation can be used to rewrite (A.1) as

$$n\,\mathbb{P}\left(\left(\frac{R}{b(n)}, \boldsymbol{\omega}\right) \in \cdot\right) \xrightarrow{v} \nu_{\alpha} \times S_{\boldsymbol{X}}\,, \tag{A.3}$$

where $S_{\boldsymbol{X}} := \sum_{u\in V} \|b_u\|_2^{\alpha} \delta_{\bar{b_u}}(\boldsymbol{\omega})$ is the spectral, or angular, measure defined on Borel subsets,

[7] A measure on the cone $\mathbb{C}$ is called Radon if it is finite for all dense subsets in the Borel space.

with $\bar{b_u} := \frac{b_u}{\|b_u\|_2}$ being the normalized vector, and $\delta_{\bar{b}_u}(\boldsymbol{\omega})$ the Dirac delta function. Hence, the dependence of $\boldsymbol{X} \in \text{MRV}_\alpha^d$ can be represented by the spectral measure on the $(d-1)$-dimensional unit ball.

A.2 Squared scaling estimation

As mentioned in Section 5.1, one way to estimate the squared scalings σ^2 is through the discrete spectral measure $S_{\boldsymbol{X}}$. First, we investigate the total mass of the spectral measure on $\boldsymbol{\Theta}_{d-1}$, which is

$$\begin{aligned} S_{\boldsymbol{X}}\left(\boldsymbol{\Theta}_{d-1}\right) &= \int_{\boldsymbol{\Theta}_{d-1}} \mathrm{d}S(\boldsymbol{\omega}) \\ &= \int_{\boldsymbol{\Theta}_{d-1}} \sum_{u \in V} \omega_i^2 \, \mathrm{d}S(\boldsymbol{\omega}) \\ &= \sum_{u \in V} \int_{\boldsymbol{\Theta}_{d-1}} \omega_i^2 \, \mathrm{d}S(\boldsymbol{\omega}) \\ &= \sum_{u \in V} \sigma_{X_u}^2 \,. \end{aligned} \tag{A.4}$$

Hence, we can define a new probability measure $\tilde{S}_{\boldsymbol{X}} := \frac{S_{\boldsymbol{X}}(\cdot)}{S_{\boldsymbol{X}}(\boldsymbol{\Theta}_{d-1})}$, which is the standardized spectral measure on $\boldsymbol{\Theta}_{d-1}$.

This probability measure is particularly useful as it allows to estimate the scalings through polar coordinates. Specifically, let $\boldsymbol{X}_i \in \text{MRV}_\alpha^d$ such that we can define $R_i = \|\boldsymbol{X}_i\|$ and $\boldsymbol{\omega}_i = \frac{\boldsymbol{X}_i}{R_i}$, for $i = 1, \ldots, n$. When choosing the inverse function $b^{\leftarrow}(x) = \mathbb{P}\left(R > x\right)^{-1}$, Resnick (2007) shows that the limiting probability in (A.2) can be rewritten as

$$\mathbb{P}\left(\frac{R}{x} > 1 \cap \boldsymbol{\omega} \in \cdot\right) = \mathbb{P}\left(\boldsymbol{\omega} \in \cdot \mid R > x\right) \xrightarrow{v} S_{\boldsymbol{X}}(\cdot) \qquad x \to \infty \,.$$

Hence, the new probability measure $\tilde{S}_{\boldsymbol{X}}$ is obtained in the limit when rescaling the inverse function as $\frac{b^{\leftarrow}(x)}{S_{\boldsymbol{X}}(\boldsymbol{\Theta}_{d-1})}$. Klüppelberg and Krali (2021) use this result to derive an estimator at a high threshold of the radius component. To see this, define a continuous function $f : \boldsymbol{\Theta}_{d-1} \to \mathbb{R}$, such that the expected value given the empirical spectral measure can be written as

$$\hat{\mathbb{E}}_{\tilde{S}_{\boldsymbol{X}}}\left[f(\boldsymbol{\omega})\right] = \frac{1}{N_n} \sum_{i=1}^{n} f(\boldsymbol{\omega}_i) \mathbb{1}\{R_i > x\} \,, \tag{A.5}$$

where $N_n := \sum_{i=1}^n \mathbb{1}\{R_i > x\}$.

To link this estimator to the squared scalings, an appropriate function must be chosen. Following Klüppelberg and Krali (2021), the function $f(\boldsymbol{\omega}) = d \bigvee_{u \in \boldsymbol{h}} \omega_u^2$ is chosen, such that

the expectation of this function with respect to the new probability measure is given by

$$\begin{aligned}\mathbb{E}_{\tilde{S}_{\boldsymbol{X}}}\left[f(\boldsymbol{\omega})\right] &= \int_{\boldsymbol{\Theta}_{d-1}} d \bigvee_{u\in\boldsymbol{h}} \omega_u^2 \,\mathrm{d}\tilde{S}_{\boldsymbol{X}}(\boldsymbol{\omega}) \\ &= \int_{\boldsymbol{\Theta}_{d-1}} \bigvee_{u\in\boldsymbol{h}} \omega_u^2 \,\mathrm{d}S_{\boldsymbol{X}}(\boldsymbol{\omega}) \\ &= \int_{\boldsymbol{\Theta}_{d-1}} \sum_{v\in V} \bigvee_{u\in\boldsymbol{h}} \omega_u^2 \|b_v\|_2^2 \delta_{\bar{b_v}}(\boldsymbol{\omega}) \\ &= \sum_{v\in V} \bigvee_{u\in\boldsymbol{h}} b_{uv}^2 \,,\end{aligned} \tag{A.6}$$

which is equal to the squared scalings as defined in Section 3.4. Hence, by using this particular function, the scalings can be estimated as

$$\hat{\sigma}^2_{M_{\boldsymbol{h}}} = \frac{d}{N_n} \sum_{i=1}^{n} \bigvee_{u\in\boldsymbol{h}} \omega_{ui}^2 \mathbb{1}\{R_i > x\} \,. \tag{A.7}$$

We refer to Klüppelberg and Krali (2021) for further asymptotic properties of the estimator.

B Illustrative examples

Example B.1. Inspired by the examples of Gissibl and Klüppelberg (2018), consider a recursive ML model $\boldsymbol{X} = (X_1, X_2, X_3, X_4)$ on a DAG $\mathcal{D}$ with

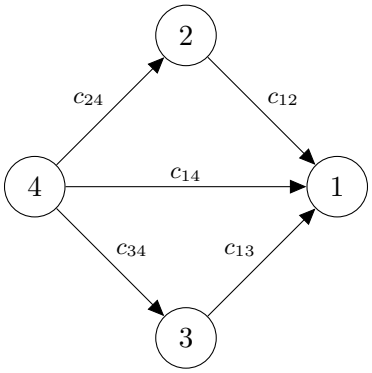

Using the max-linear equation model in (3.2), we can write the components of $\boldsymbol{X}$ as

$$
\begin{aligned}
X_4 &= c_{44}\varepsilon_4 \\
X_3 &= c_{33}\varepsilon_3 \vee c_{34}X_4 \\
&= c_{33}\varepsilon_3 \vee c_{34}c_{44}\varepsilon_4 \\
X_2 &= c_{22}\varepsilon_2 \vee c_{24}X_4 \\
&= c_{22}\varepsilon_2 \vee c_{24}c_{44}\varepsilon_4 \\
X_1 &= c_{11}\varepsilon_1 \vee c_{12}X_2 \vee c_{13}X_3 \vee c_{14}X_4 \\
&= c_{11}\varepsilon_1 \vee c_{12}c_{22}\varepsilon_2 \vee c_{13}c_{33}\varepsilon_3 \vee (c_{12}c_{24}c_{44} \vee c_{13}c_{34}c_{44})\varepsilon_4
\end{aligned}
$$

Hence $\boldsymbol{X}$ is a ML model with ML coefficient matrix B

$$
B = \begin{pmatrix}
c_{11} & c_{12}c_{22} & c_{13}c_{33} & c_{12}c_{24}c_{44} \vee c_{13}c_{34}c_{44} \\
0 & c_{22} & 0 & c_{24}c_{44} \\
0 & 0 & c_{33} & c_{34}c_{44} \\
0 & 0 & 0 & c_{44}
\end{pmatrix}.
$$

C Algorithms

Algorithm C.1 Identifying the initial vertices

Input: $\boldsymbol{X} \in \mathbb{R}^d; z_1, z_2 > 0; a > 1$
  Initialize: $\boldsymbol{\phi}, \boldsymbol{\tau} := (0)_{d\times 1}$

  for $i = d$ to 1 **do**
    $\boldsymbol{\phi}_i = \hat{\sigma}^2_{M_{-i,ai}} - \hat{\sigma}^2_{M_V} - a^2 + 1$
    if $z_1 \leq \boldsymbol{\phi}_i \leq z_2$ **then**
      $\boldsymbol{\theta}_i = i$
  return $\boldsymbol{\theta}$

Note that z_1 and z_2 are treated as the lower and upper estimation bounds. Similar to Klüppelberg and Krali (2021), the values are set to $a = \sqrt{2}$, $z_1 = 0.1$ and $z_2 = 0.05$.

Algorithm C.2 Identifying the $(h+1)$-th vertex

Input: $\boldsymbol{X} \in \mathbb{R}^d; z_3 > 0; a, h > 1; \pi : \mathbb{R}^{d\times d} \to \mathbb{R}^{d\times d}$
  Initialize: $\boldsymbol{\phi}, \boldsymbol{\tau} := (0)_{d\times 1}; \boldsymbol{h} := \left\{\pi^{-1}(d), \ldots, \pi^{-1}(d-h+1)\right\}$

  for $i \notin \boldsymbol{h}$ **do**
    $k := \boldsymbol{h} \cup \{i\}$
    $\boldsymbol{\phi}_i = \hat{\sigma}^2_{M_{\boldsymbol{h}_a, i_a, k^c}} - \hat{\sigma}^2_{M_V} - (a^2-1)\hat{\sigma}^2_{M_{\boldsymbol{h}_a, i}}$
    if $|\boldsymbol{\phi}_i| \leq z_3$ **then**
      $\boldsymbol{\theta}_i = i$
  return $\boldsymbol{\theta}$

Instead of the two estimation bounds in Algorithm C.1, this algorithm considers a single bound z_3. Similarly, the values are set to $a = \sqrt{2}$ and $z_3 = 0.1$.

D Additional descriptive statistics

Table D.1: Historical information about the included U.S. banks.
This table reports historical information about the 30 U.S. banks that are used in this research. Reported are the ticker on the NYSE, the legal name of the bank, its founding year, and location of the headquarters, respectively. The headquarters refer to the location where the bank was legally registered the longest during the sample period. Founding years with an asterisk indicate banks that no longer exist. The reported information is retrieved from the official website of each bank.

Ticker	Legal name	Founding year	Headquarters
AB	Alliancebernstein Holding LP	1967	New York City (NY)
ASB	Associated Banc-Corp.	1861	Green Bay (WI)
BAC	Bank of America	1928	Charlotte (NC)
BEN	Franklin Templeton	1947	San Mateo (CA)
BK	Bank of New York Mellon	1784	Manhatten (NY)
BOH	Bank of Hawaii	1897	Honolulu (HI)
BXS	BancorpSouth	1876	Tupelo (MS)
CBU	Community Bank	1866	DeWitt (NY)
CFR	Cullen/Frost Bankers	1868	San Antonio (TX)
CMA	Comerica	1849	Dallas (TX)
CPF	Central Pacific Financial Corp.	1954	Honolulu (HI)
EV	Eaton Vance	1979	Boston (MA)
FHN	First Horizon National Corp.	1864	Memphis (TN)
FNB	F.N.B. Corp.	1864	Pittsburgh (PA)
JEF	Jefferies Financial Group	1968	New York City (NY)
JPM	JPMorgan Chase & Co.	1799	New York City (NY)
KEY	KeyCorp.	1825	Albany (NY)
LM	Legg Mason	1899*	Baltimore (MD)
MTB	M&T Bank Corp.	1856	Buffalo (NY)
PNC	PNC Financial Services Group	1845	Pittsburgh (PA)
RF	Regions Financial Corp.	1971	Birmingham (AL)
RJF	Raymond James Financial	1962	St. Petersburg (FL)
SCHW	Charles Schwab Corp.	1971	San Francisco (CA)
SF	Stifel Financial Corp.	1890	Saint Louis (MO)
SFE	Safeguard Scientifics	1953	Radnor (PA)
SNV	Synovus Financial Corp.	1888	Columbus (GA)
TFC	Truist Financial Corp.	1872	Charlotte (NC)
USB	U.S. Bancorp	1968	Minneapolis (MN)
WBS	Webster Financial Corp.	1935	Waterbury (CT)
WFC	Wells Fargo & Co	1852	San Francisco (CA)

Table D.2: Summary statistics for negative daily equity returns.
This table reports summary statistics for daily stock returns over the sample period January 2, 1990 to December 31, 2014. Only negative returns are considered, such that this table focusses on the left tail of the distribution. Reported are the mean, standard deviation (Std. dev.), minimum (Min.), maximum (Max.), median (Median) and the number of observations (Obs), respectively. Daily stock return data is based on data from Datastream. There are 30 banks included in the analysis. All values except the number of observations are in percentages. The list consists of all banks that are preliminary traded on the NYSE during the sample period. Further information regarding the bank names and historical context is given in Table D.1 in Appendix D.

Bank	Mean	Std. dev.	Min.	Max.	Median	Obs.
AB	−1.625	1.709	−20.637	−0.013	−1.156	2,857
ASB	−1.521	1.622	−18.999	−0.024	−1.072	2,806
BAC	−1.696	2.285	−34.206	−0.010	−1.058	3,012
BEN	−1.612	1.622	−16.577	−0.008	−1.130	2,969
BK	−1.577	1.764	−31.687	−0.019	−1.089	3,020
BOH	−1.251	1.403	−25.508	−0.017	−0.846	2,876
BXS	−1.689	1.669	−17.575	−0.030	−1.215	2,719
CBU	−1.586	1.566	−14.221	−0.021	−1.122	2,667
CFR	−1.384	1.451	−21.457	−0.016	−0.993	2,857
CMA	−1.466	1.732	−22.694	−0.016	−0.972	2,952
CPF	−2.394	2.748	−43.570	−0.023	−1.637	2,734
EV	−1.730	1.741	−19.835	−0.024	−1.253	2,809
FHN	−1.579	2.070	−44.114	−0.021	−1.010	2,862
FNB	−1.893	2.132	−25.533	−0.029	−1.223	2,572
JEF	−1.382	1.601	−23.233	−0.020	−0.919	2,869
JPM	−1.682	1.819	−23.228	−0.017	−1.163	3,006
KEY	−1.646	2.234	−40.547	−0.027	−1.028	2,867
LM	−1.748	2.004	−28.438	−0.010	−1.182	2,894
MTB	−1.108	1.346	−16.972	−0.009	−0.697	2,904
PNC	−1.471	1.840	−53.436	−0.013	−1.002	2,946
RF	−1.663	2.457	−52.885	−0.027	−0.988	2,853
RJF	−1.774	1.804	−26.118	−0.018	−1.253	2,901
SCHW	−2.093	1.965	−21.123	−0.035	−1.514	3,061
SF	−1.811	1.679	−27.112	−0.018	−1.419	2,598
SFE	−2.768	2.921	−29.728	−0.050	−1.887	2,985
SNV	−1.870	2.228	−30.069	−0.029	−1.236	2,804
TFC	−1.443	1.599	−26.608	−0.023	−0.993	2,821
USB	−1.443	1.687	−20.047	−0.022	−0.979	2,809
WBS	−1.763	2.045	−23.511	−0.020	−1.221	2,828
WFC	−1.469	1.749	−27.210	−0.015	−0.976	2,942

Table D.3: Shape parameters and tail indexes for sample distributions of daily equity returns.
This table reports the shape parameters and tail indexes for the sample distributions of the U.S. banks daily equity returns over the sample period January 2, 1990 to December 31, 2014. The shape parameter ξ belongs to the generalized Pareto distribution, and the tail index α is its reciprocal value. Further information about the banks and historical context is given Table D.1 in Appendix D.

	both tails		*left tail*		*right tail*	
Bank	$\hat{\xi}$	$\hat{\alpha}$	$\hat{\xi}$	$\hat{\alpha}$	$\hat{\xi}$	$\hat{\alpha}$

Table D.3: Shape parameters and tail indexes for sample distributions of daily equity returns.
This table reports the shape parameters and tail indexes for the sample distributions of the U.S. banks daily equity returns over the sample period January 2, 1990 to December 31, 2014. The shape parameter ξ belongs to the generalized Pareto distribution, and the tail index α is its reciprocal value. Further information about the banks and historical context is given Table D.1 in Appendix D.

	both tails		*left tail*		*right tail*	
Bank	$\hat{\xi}$	$\hat{\alpha}$	$\hat{\xi}$	$\hat{\alpha}$	$\hat{\xi}$	$\hat{\alpha}$
AB	0.215	4.662	0.330	3.030	0.310	3.227
	(0.094)		(0.031)		(0.030)	
ASB	0.237	4.211	0.293	3.415	0.310	3.227
	(0.067)		(0.036)		(0.029)	
BAC	0.328	3.048	0.394	2.537	0.406	2.465
	(0.032)		(0.025)		(0.023)	
BEN	0.228	4.384	0.258	3.872	0.317	3.157
	(0.076)		(0.056)		(0.031)	
BK	0.287	3.481	0.314	3.184	0.354	2.823
	(0.041)		(0.034)		(0.027)	
BOH	0.283	3.535	0.314	3.188	0.337	2.967
	(0.043)		(0.035)		(0.026)	
BXS	0.191	5.245	0.262	3.81	0.273	3.659
	(0.149)		(0.040)		(0.034)	
CBU	0.254	3.943	0.307	3.262	0.352	2.842
	(0.056)		(0.029)		(0.021)	
CFR	0.284	3.526	0.295	3.392	0.341	2.934
	(0.042)		(0.037)		(0.026)	
CMA	0.302	3.314	0.367	2.727	0.354	2.823
	(0.037)		(0.027)		(0.026)	
CPF	0.252	3.965	0.364	2.746	0.370	2.701
	(0.057)		(0.022)		(0.021)	
EV	0.275	3.643	0.275	3.631	0.330	3.029
	(0.046)		(0.041)		(0.026)	
FHN	0.288	3.474	0.380	2.633	0.372	2.686

Table D.3: Shape parameters and tail indexes for sample distributions of daily equity returns.
This table reports the shape parameters and tail indexes for the sample distributions of the U.S. banks daily equity returns over the sample period January 2, 1990 to December 31, 2014. The shape parameter ξ belongs to the generalized Pareto distribution, and the tail index α is its reciprocal value. Further information about the banks and historical context is given Table D.1 in Appendix D.

	both tails		*left tail*		*right tail*	
Bank	$\hat{\xi}$	$\hat{\alpha}$	$\hat{\xi}$	$\hat{\alpha}$	$\hat{\xi}$	$\hat{\alpha}$
	(0.041)		(0.025)		(0.023)	
FNB	0.259	3.863	0.33	3.031	0.355	2.818
	(0.053)		(0.024)		(0.020)	
JEF	0.234	4.279	0.335	2.989	0.355	2.814
	(0.071)		(0.029)		(0.024)	
JPM	0.285	3.511	0.295	3.392	0.336	2.977
	(0.042)		(0.040)		(0.029)	
KEY	0.367	2.724	0.405	2.466	0.418	2.392
	(0.026)		(0.023)		(0.020)	
LM	0.258	3.877	0.368	2.719	0.312	3.203
	(0.053)		(0.025)		(0.030)	
MTB	0.339	2.950	0.371	2.692	0.368	2.715
	(0.030)		(0.027)		(0.024)	
PNC	0.281	3.556	0.325	3.075	0.357	2.803
	(0.043)		(0.032)		(0.026)	
RF	0.388	2.580	0.463	2.162	0.471	2.124
	(0.024)		(0.020)		(0.018)	
RJF	0.264	3.783	0.296	3.383	0.282	3.548
	(0.050)		(0.038)		(0.037)	
SCHW	0.213	4.704	0.241	4.147	0.240	4.166
	(0.097)		(0.059)		(0.063)	
SF	0.240	4.161	0.295	3.392	0.320	3.122
	(0.065)		(0.028)		(0.028)	
SFE	0.274	3.647	0.295	3.386	0.286	3.491
	(0.046)		(0.032)		(0.038)	
SNV	0.294	3.400	0.378	2.642	0.384	2.605
	(0.038)		(0.023)		(0.021)	
TFC	0.288	3.471	0.315	3.178	0.358	2.793
	(0.041)		(0.021)		(0.023)	
USB	0.291	3.434	0.354	2.822	0.351	2.849
	(0.040)		(0.029)		(0.024)	
WBS	0.262	3.815	0.354	2.828	0.336	2.979

Table D.3: Shape parameters and tail indexes for sample distributions of daily equity returns.
This table reports the shape parameters and tail indexes for the sample distributions of the U.S. banks daily equity returns over the sample period January 2, 1990 to December 31, 2014. The shape parameter ξ belongs to the generalized Pareto distribution, and the tail index α is its reciprocal value. Further information about the banks and historical context is given Table D.1 in Appendix D.

	both tails		*left tail*		*right tail*	
Bank	$\hat{\xi}$	$\hat{\alpha}$	$\hat{\xi}$	$\hat{\alpha}$	$\hat{\xi}$	$\hat{\alpha}$
	(0.051)		(0.026)		(0.026)	
WFC	0.300	3.329	0.347	2.879	0.402	2.488
	(0.037)		(0.029)		(0.022)	

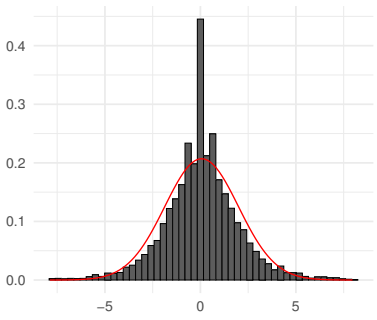

AB

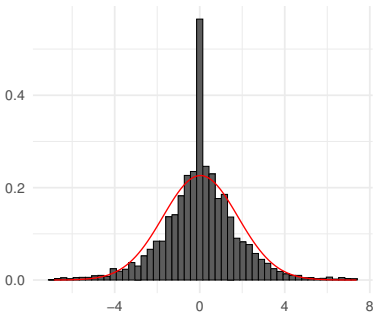

ASB

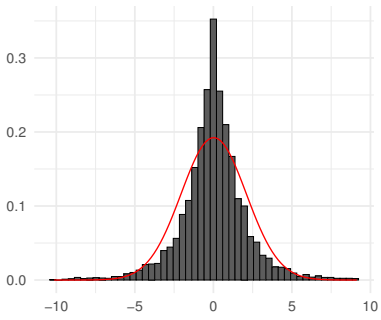

BAC

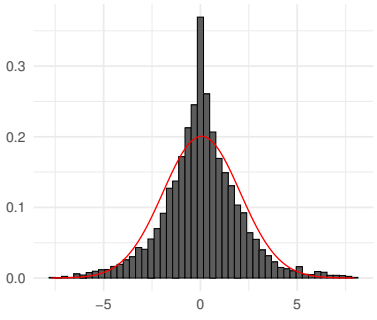

BEN

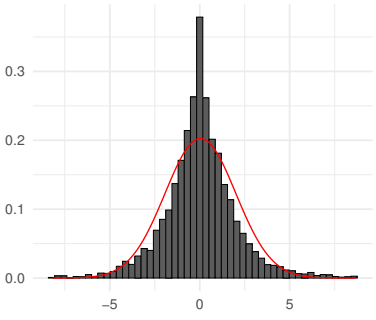

BK

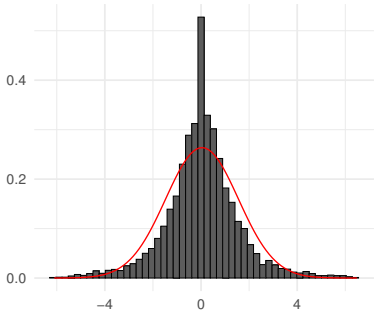

BOH

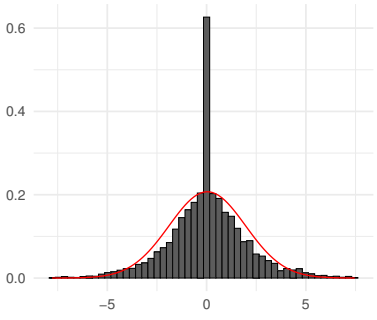

BXS

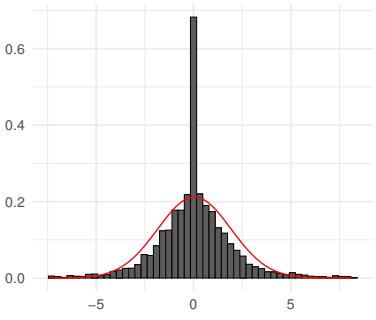

CBU

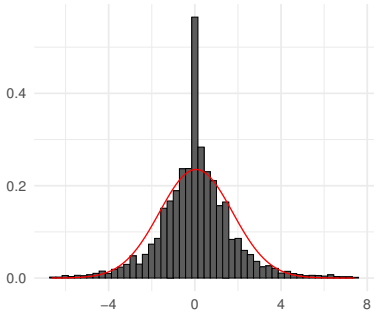

CFR

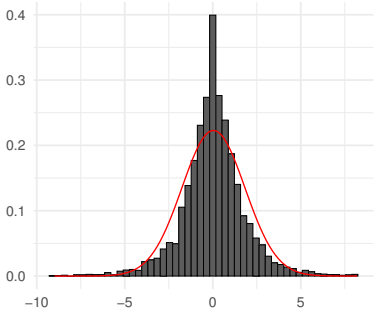

CMA

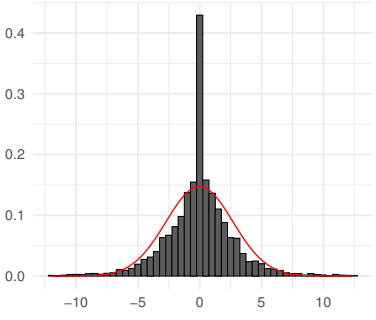

CPF

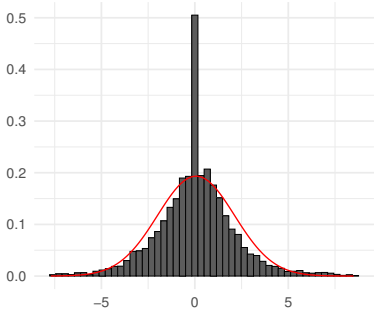

EV

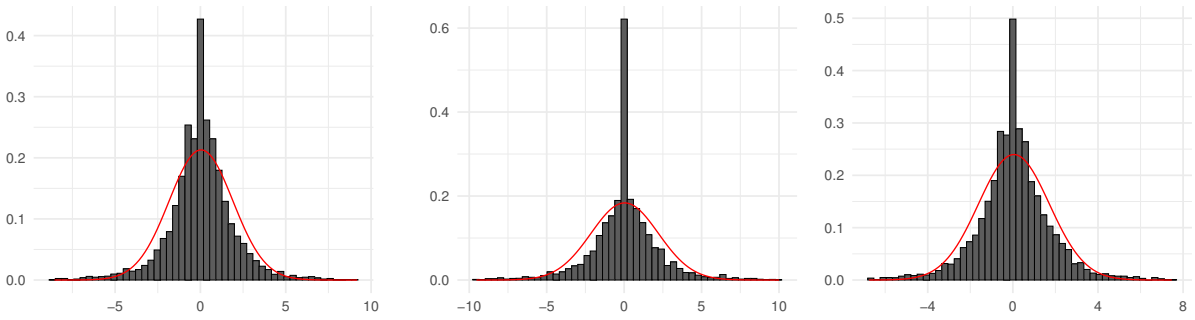

FHN

FNB

JEF

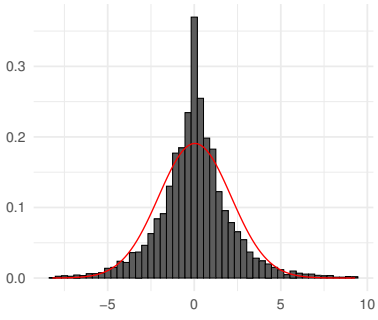

JPM

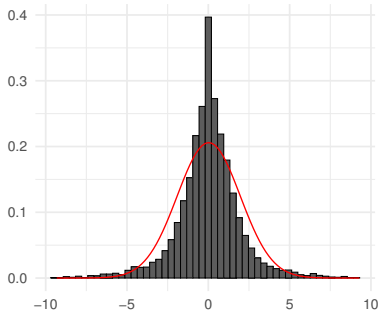

KEY

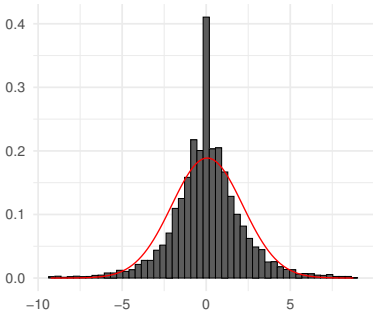

LM

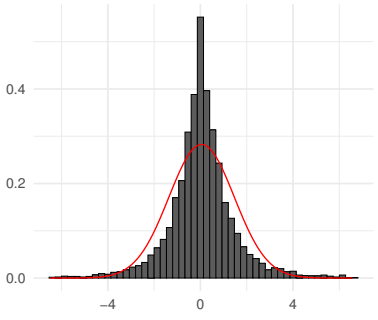

MTB

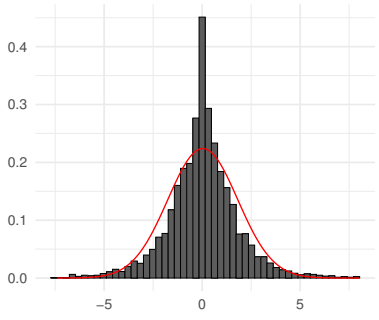

PNC

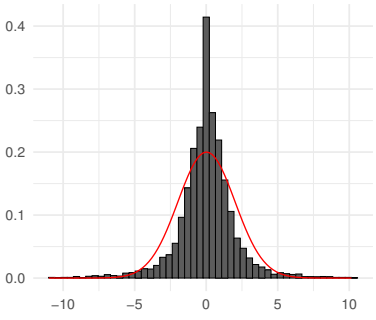

RF

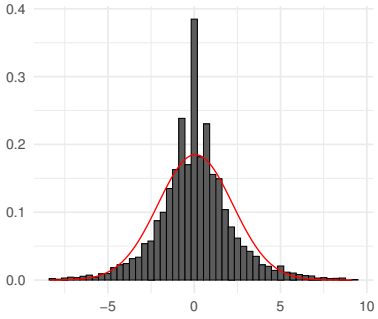

RJF

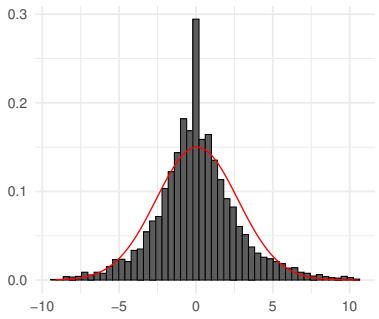

SCHW

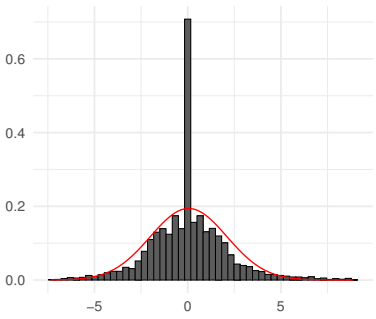

SF

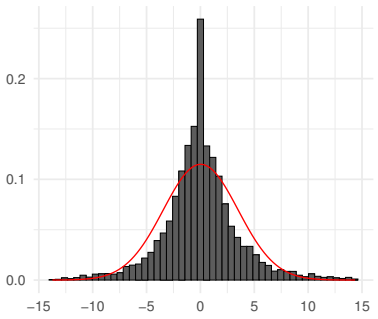

SFE

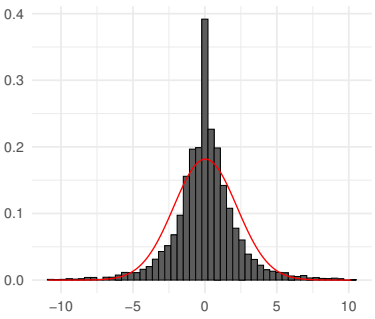

SNV

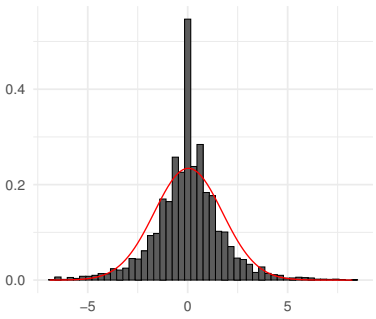

TFC

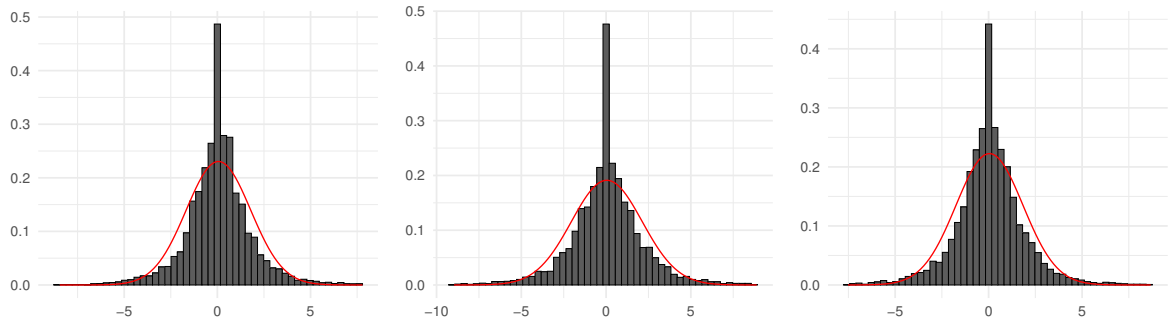

Figure D.1: Histograms of the daily stock returns. These returns are constructed by applying log transformations on the return index, and taking first differences for each bank. The full name of each bank is provided in Table 2 in Appendix E. The red line represents a fitted normal distribution based on the sample mean and standard deviation. Samples are cut off at the 0.5th and 99.5th percentiles for visual clarity.

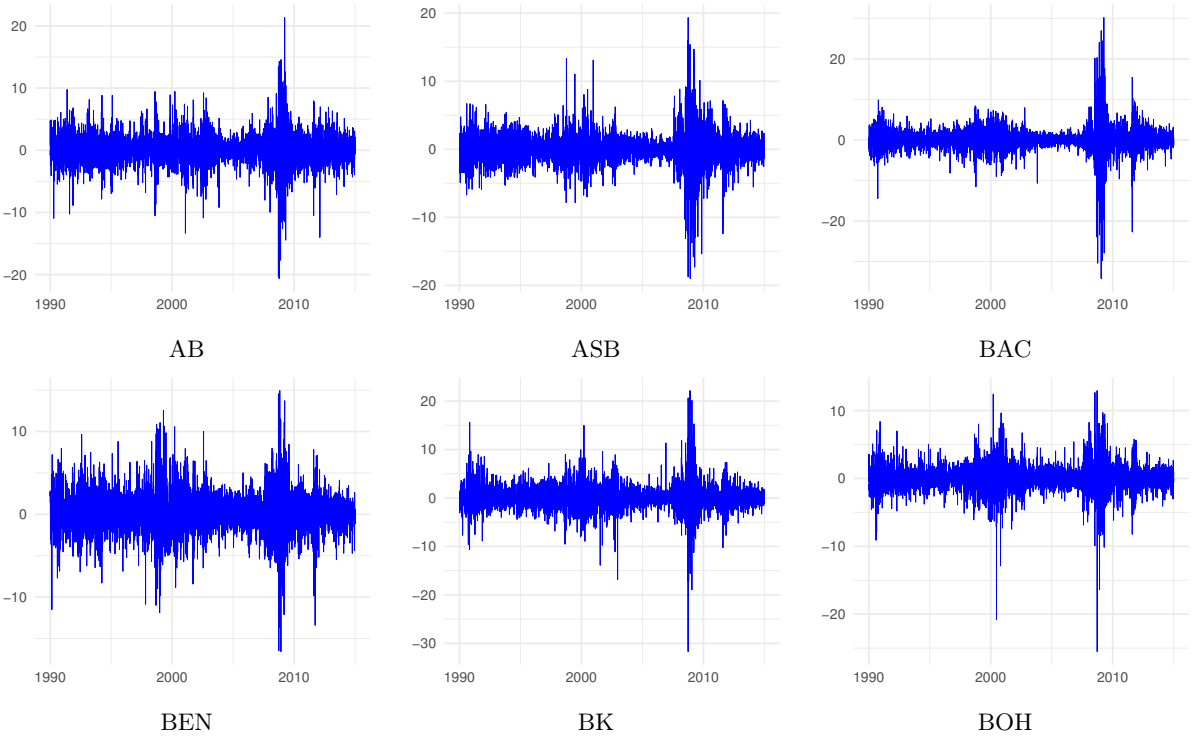

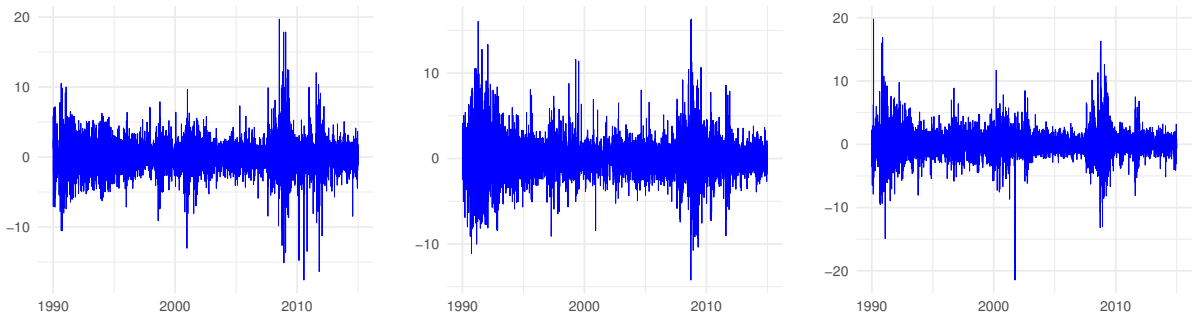

BXS

CBU

CFR

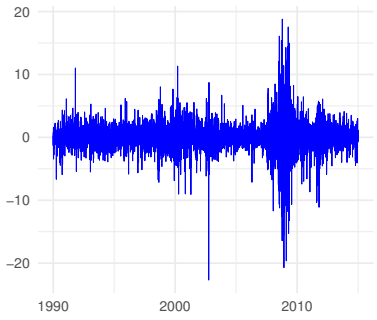

CMA

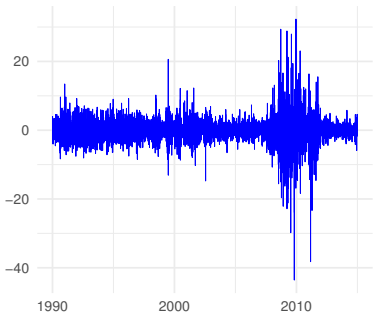

CPF

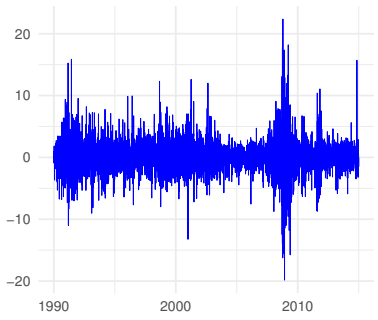

EV

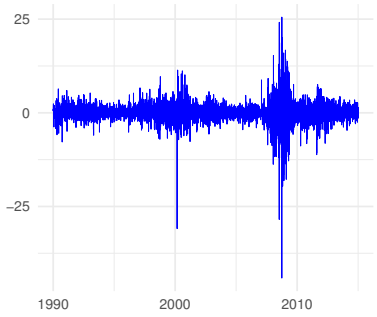

FHN

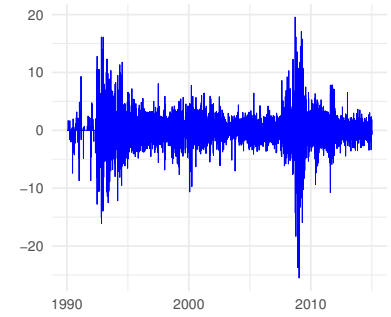

FNB

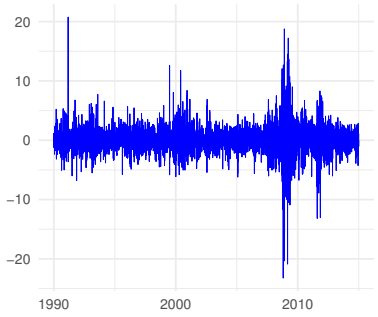

JEF

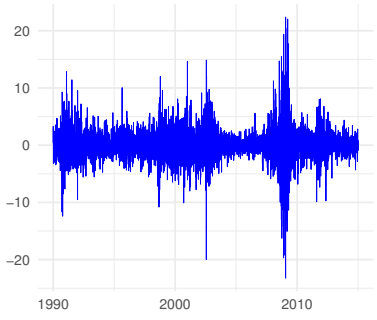

JPM

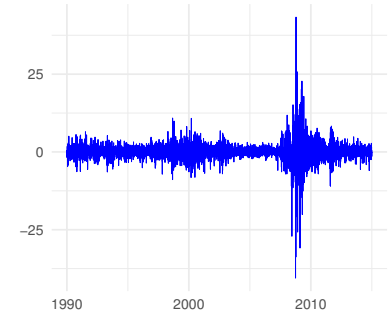

KEY

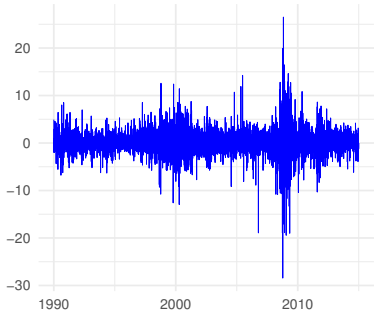

LM

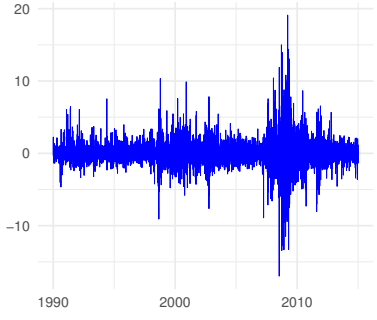

MTB

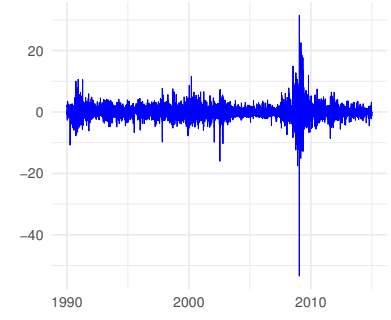

PNC

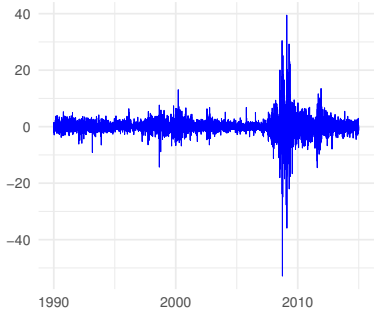

RF

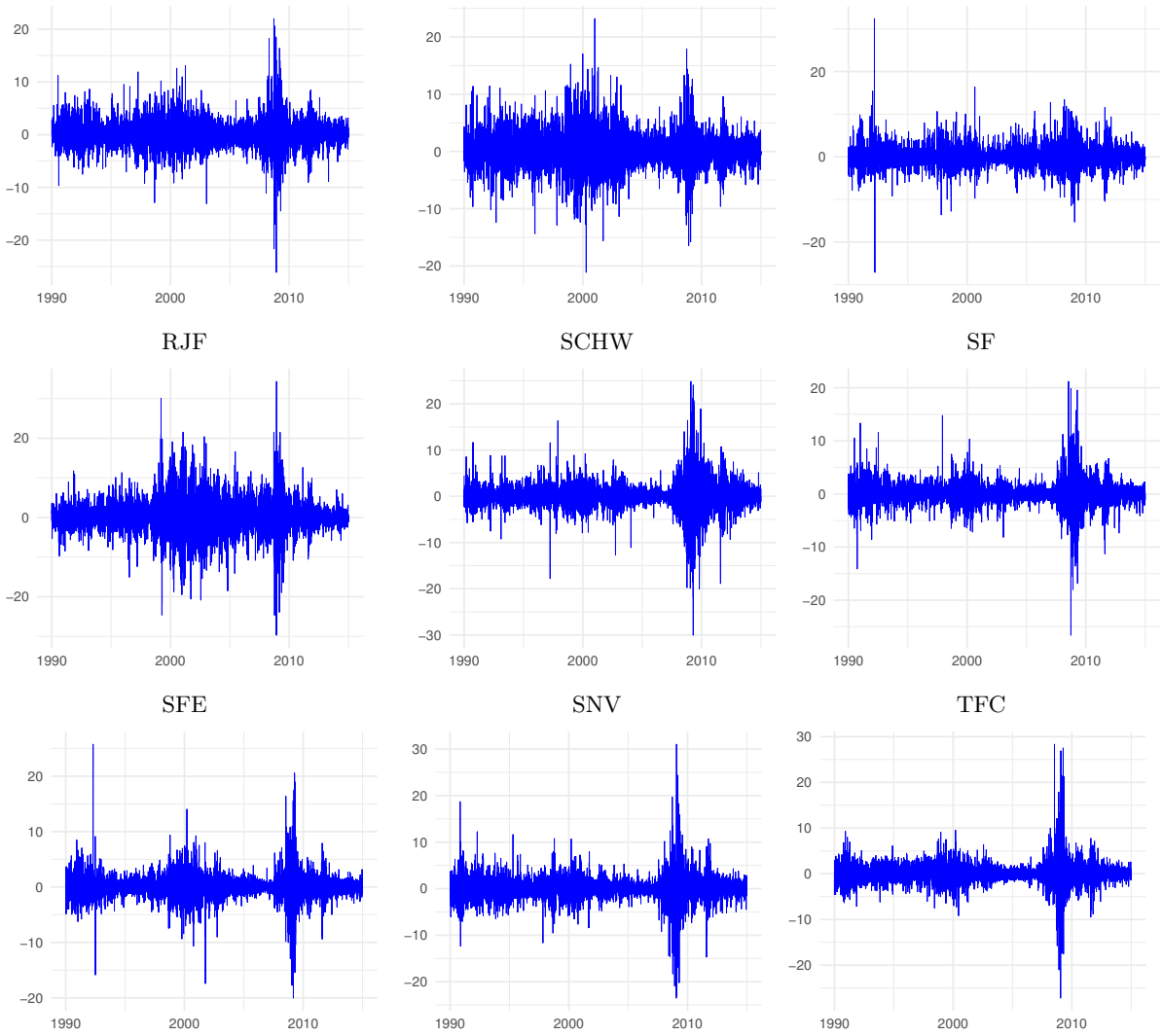

Figure D.2: Daily equity returns of 30 U.S. banks over the sample period January 2, 1990 to December 31, 2014. These returns are constructed by applying log transformations on the return index, and taking first differences for each bank. The full name of each bank is provided in Table 2 in Appendix E.

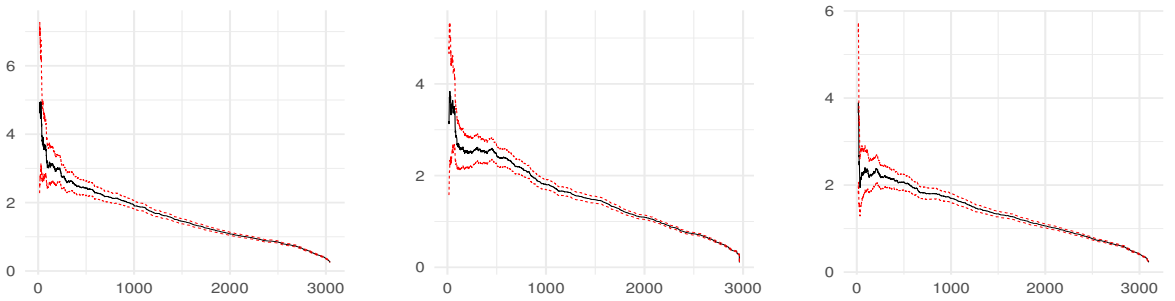

AB ASB BAC

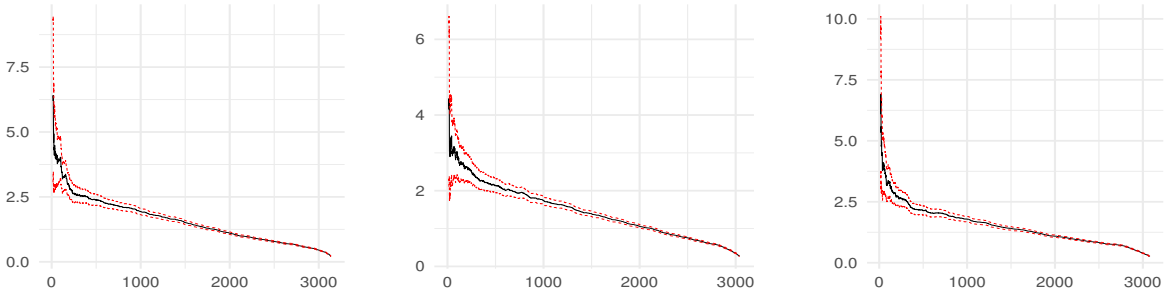

BEN BK BOH

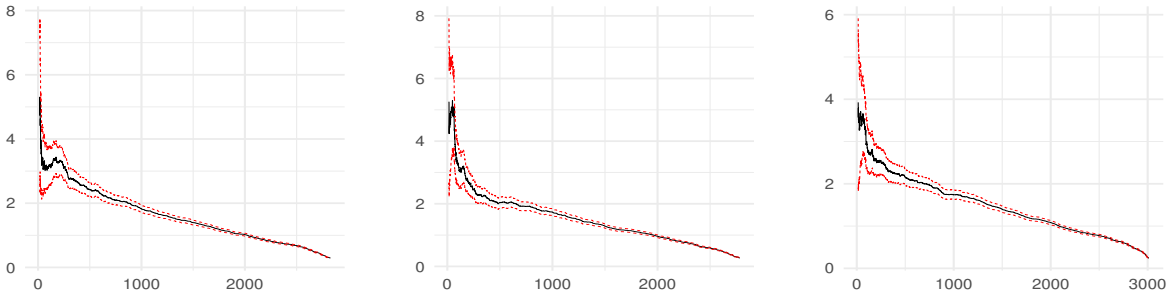

BXS CBU CFR

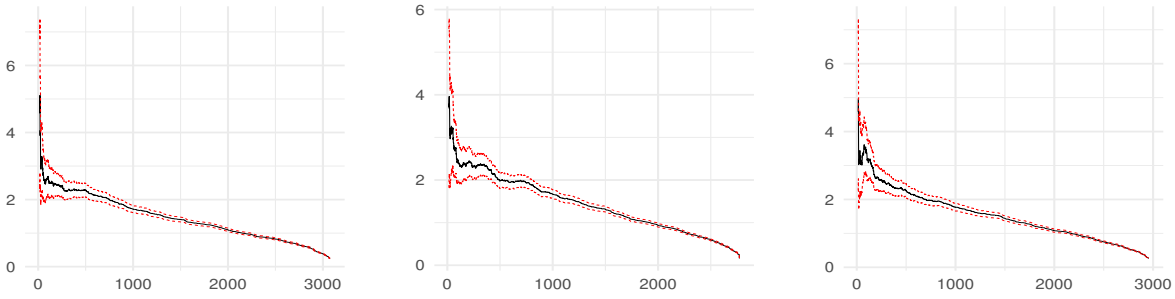

CMA CPF EV

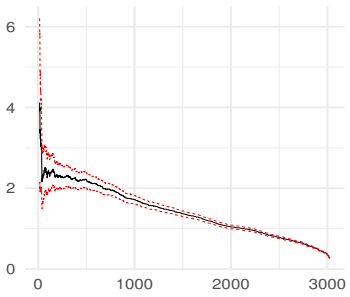

FHN

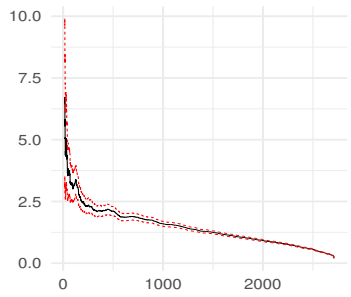

FNB

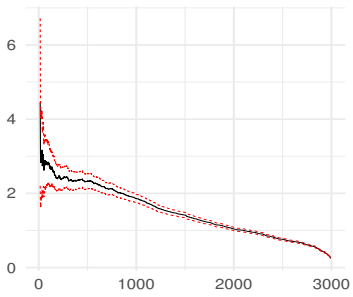

JEF

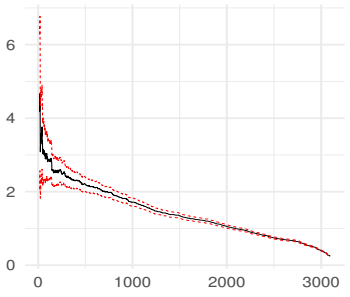

JPM

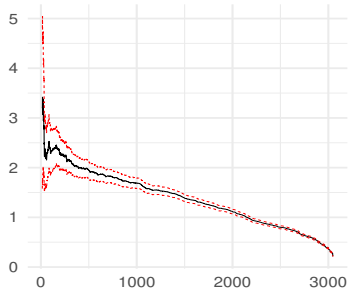

KEY

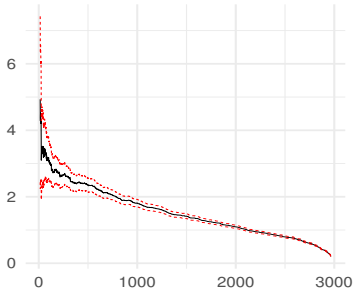

LM

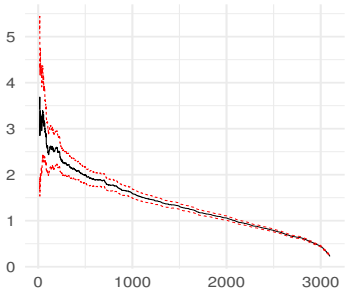

MTB

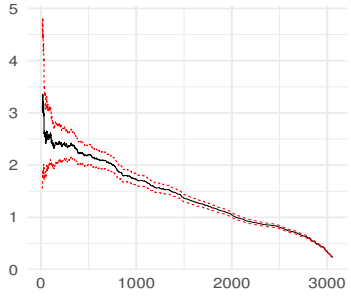

PNC

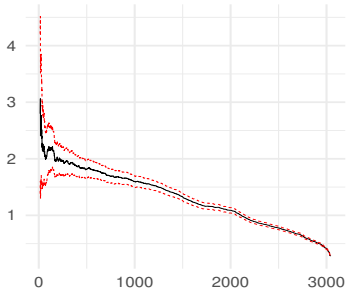

RF

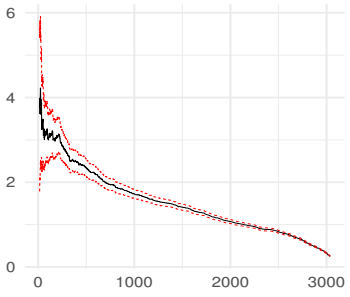

RJF

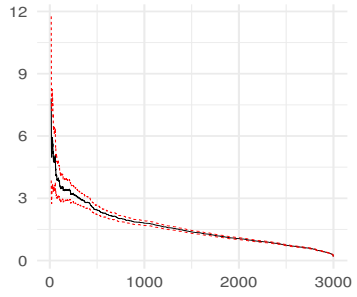

SCHW

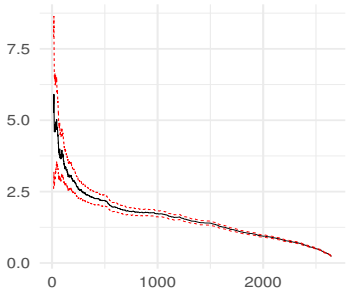

SF

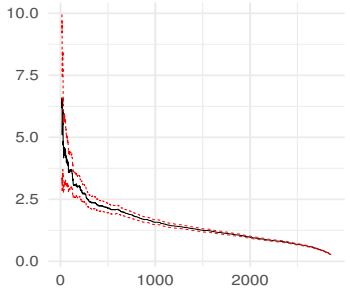

SFE

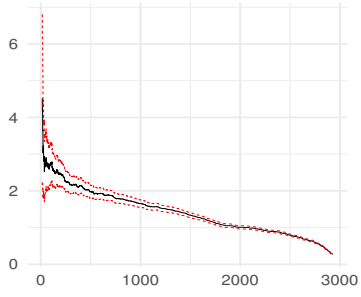

SNV

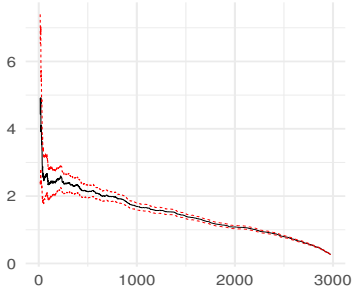

TFC

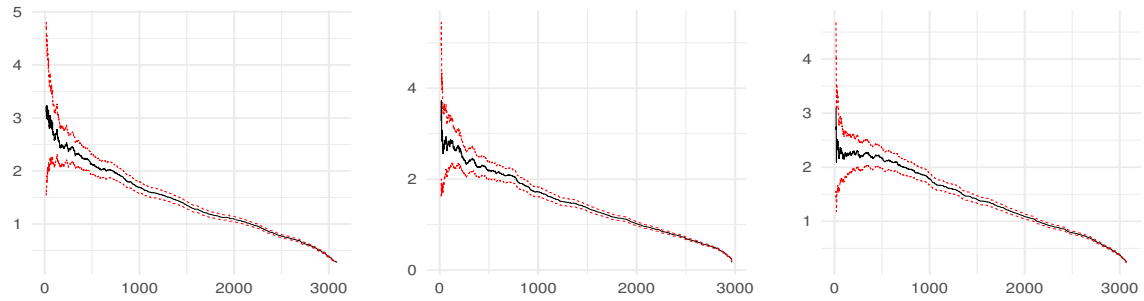

USB WBS WFC

Figure D.3: Hill plots of the daily stock returns. These returns are constructed by applying log transformations on the return index, and taking first differences for each bank. The full name of each bank is provided in Table 2 in Appendix E. The red lines represent a 95% confidence interval.

E Additional results

Table E.1: Correlation between size and centrality using weekly returns.
This table reports correlation values between size and centrality over the sample period January 2, 1990 to December 31, 2014. Weekly returns are used to calculate the centrality measures. Size corresponds to total assets, debt and equity, whereas centrality entails the in- and out-degree and the causal order (Rank). Accounting data is based on data from Datastream. The centrality measures are obtained by employing Algorithm C.1 and C.2. Reported are the Pearson, Spearman, and Kendall correlation. Significance at the 10%-, 5%-, and 1%-level are indicated by *, **, and ***, respectively.

	In-degree	Out-degree	Rank
Panel A: Pearson			
Total assets	0.045*	−0.032*	−0.039*
Total debt	0.053*	−0.046	−0.045*
Total equity	0.044	−0.028*	−0.039*
Panel B: Spearman			
Total assets	−0.030**	0.080***	0.066***
Total debt	−0.018	0.065***	0.055***
Total equity	−0.009	0.078***	0.050***
Panel C: Kendall			
Total assets	−0.019**	0.055***	0.044***
Total debt	−0.012	0.044***	0.036***
Total equity	−0.007	0.054***	0.034***

Table E.2: Correlation between systemic importance and centrality using weekly returns.
This table reports correlation values between systemic importance measures and centrality over the sample period January 2, 1990 to December 31, 2014. Reported are both the systemic importance measures PAO, VI and SII assets, debt and equity, and centrality indicators in- and out-degree and the causal order (Rank). Weekly returns are used to calculate all measures in this table. Accounting data is based on data from Datastream. The centrality measures are obtained by employing Algorithm C.1 and C.2. Reported are the Pearson, Spearman, and Kendall correlation. Significance at the 10%-, 5%-, and 1%-level are indicated by *, **, and ***, respectively.

	In-degree	Out-degree	Rank
Panel A: Pearson			
PAO	−0.071***	0.046***	0.079***
VI	0.013	−0.038***	0.027**
SII	−0.013	0.064***	0.063***
Panel B: Spearman			
PAO	−0.081***	0.064***	0.085***
VI	0.011*	−0.066***	0.030**
SII	−0.004	0.097***	0.060***
Panel C: Kendall			
PAO	−0.064***	0.050***	0.067***
VI	0.008	−0.046***	0.020**
SII	−0.004	0.068***	0.042***

Table E.3: Correlation between size and centrality using excess returns.
This table reports correlation values between size and centrality over the sample period January 2, 1990 to December 31, 2014. Excess returns are constructed by subtracting 3-month LIBOR rates from the original series. Size corresponds to total assets, debt and equity, whereas centrality entails the in- and out-degree and the causal order (Rank). Accounting data is based on data from Datastream. The centrality measures are obtained by employing Algorithm C.1 and C.2. Reported are the Pearson, Spearman, and Kendall correlation. Significance at the 10%-, 5%-, and 1%-level are indicated by *, **, and ***, respectively.

	In-degree	Out-degree	Rank
Panel A: Pearson			
Total assets	−0.046***	0.007	0.039**
Total debt	−0.035**	0.000***	0.027*
Total equity	−0.038**	0.004	0.031**
Panel B: Spearman			
Total assets	−0.127***	0.101***	0.132***
Total debt	−0.135***	0.110***	0.141***
Total equity	−0.113	0.088***	0.115***
Panel C: Kendall			
Total assets	−0.088***	0.070***	0.092***
Total debt	−0.094***	0.076***	0.099***
Total equity	−0.077***	0.061***	0.080***

Table E.4: Correlation between systemic importance and centrality using excess returns.
This table reports correlation values between systemic importance measures and centrality over the sample period January 2, 1990 to December 31, 2014. Reported are both the systemic importance measures PAO, VI and SII assets, debt and equity, and centrality indicators in- and out-degree and the causal order (Rank). Excess returns are constructed by subtracting 3-month LIBOR rates from the original series. Accounting data is based on data from Datastream. The centrality measures are obtained by employing Algorithm C.1 and C.2. Reported are the Pearson, Spearman, and Kendall correlation. Significance at the 10%-, 5%-, and 1%-level are indicated by *, **, and ***, respectively.

	In-degree	Out-degree	Rank
Panel A: Pearson			
PAO	−0.079***	0.044***	0.098***
VI	−0.070***	0.012	0.057***
SII	−0.078***	0.030	0.090***
Panel B: Spearman			
PAO	−0.124***	0.088***	0.123***
VI	−0.077***	0.030*	0.057***
SII	−0.106	0.069***	0.102***
Panel C: Kendall			
PAO	−0.088***	0.061***	0.086***
VI	−0.054***	0.021	0.039***
SII	−0.075***	0.049***	0.072***